

UNIVERZA V LJUBLJANI
FAKULTETA ZA FARMACIJO

ŽIVA FRANGEŽ

**ŠTUDIJ ODVISNOSTI MITOHONDRIJSKE LOKALIZACIJE ATG12
OD IZRAŽANJA BCL-2**

**EVALUATION OF ATG12 MITOCHONDRIAL LOCALIZATION ON
BCL-2 EXPRESSION**

Ljubljana, 2015

The research work was carried out at the Institute of Pharmacology at the University of Bern, with collaboration of the Faculty of Pharmacy, University of Ljubljana. I worked under the supervision of Prof. Dr. Dr. Hans-Uwe Simon and home mentorship of Prof. Dr. Irena Mlinarič-Raščan.

Acknowledgments:

First, I would like to thank Prof. Dr. Dr. Hans-Uwe Simon who enabled me to perform my Master thesis at the Institute of Pharmacology, to work with his research team and take part in such an interesting project. I would like to thank him for sharing his immense knowledge with me and for all his support and guidance through the project.

I am very thankful to Dr. He Liu and Dr. Zhaoyue He who introduced and sparked my interest in the research work, for their patience and encouraging words. I would like to thank them for creating a working environment in which I always felt motivated and welcome. I am grateful for this possibility of working and learning from them. I would like to thank Dr. He Liu especially for all her advice at writing and help at correcting my thesis.

I would like to thank Prof. Dr. Irena Mlinarič-Raščan for her support and help after my return from Bern. I thank her for her professional advice at writing the thesis and preparation for my final defence.

A thank you goes also to all the members at the Institute of Pharmacology at the University of Bern for creating a working environment, in which I always felt motivated and welcome.

A special thank you goes to my family for all the support during my years of study, for their constant belief in me and all the thoughtful and reassuring words which have guided me and kept me on the right way. And lastly, a big thank you to all my friends for always being there for me, supporting me and for all the unforgettable memories. A thank you to all my classmates, »ta luštnim«, for all their help, encouraging words and the memorable times we had through all our years of study.

Statement

Hereby, I testify having performed the experiments to the best of my knowledge and having written this thesis independently under guidance of my supervisors: Prof. Dr. Irena Mlinarič-Raščan and Prof. Dr. Dr. Hans-Uwe Simon.

Ljubljana, January 2015

Živa Frangež

President of the Thesis defence committee: Assoc. Prof. Dr. Anamarija Zega

Member of the Thesis defence committee: Assist. Prof. Dr. Nina Kočevar Glavač

TABLE OF CONTENTS

TABLE OF FIGURES	V
ABSTRACT	VI
RAZŠIRJENI POVZETEK	VII
LIST OF USED ABBREVIATIONS	X
1 INTRODUCTION	1
1.1 Introduction to autophagy	1
1.2 The physiological role of autophagy	1
1.3 Autophagy in cancer.....	2
1.3.1 The role of autophagy in tumor suppression	3
1.3.2 The role of autophagy in tumor progression	4
1.4 Molecular mechanisms of autophagy.....	5
1.5 Interaction factors of Autophagy-related protein 12	8
1.5.1 Autophagy-related protein 12.....	8
1.5.2 B-cell lymphoma 2 protein (Bcl-2)	9
1.5.2.1 <i>The Bcl-2 family proteins</i>	9
1.5.2.2 <i>Interaction of ATG12 with Bcl-2</i>	10
1.5.3 Autophagy-related protein 3.....	12
1.5.4 Autophagy-related protein 5.....	13
2 OBJECTIVES	15
3 MATERIALS AND METHODS	16
3.1 Materials.....	16
3.2 Methods.....	19
3.2.1 Cell culture	19
3.2.1.1 <i>Cell passaging</i>	19
3.2.1.2 <i>Cell freezing</i>	20
3.2.1.3 <i>Cell thawing</i>	20
3.2.2 Measuring protein concentrations	21
3.2.3 Western blotting	21
3.2.4 Subcellular fractionation	23

3.2.5	Immunofluorescence staining.....	24
3.2.6	Immunohistochemistry staining	26
3.2.7	Quantification of the results from co-localization analysis	27
3.2.8	Statistical analysis	27
4	RESULTS.....	28
4.1	Mitochondrial localization of ATG12.....	28
4.2	Mitochondrial localization of ATG12 is independent on Bcl-2.....	35
4.3	Cellular expression of ATG12 in tumor and normal tissues	39
4.4	Cytosolic and mitochondrial ATG12-ATG5 conjugate	44
5	DISCUSSION	46
6	CONCLUSION.....	51
7	REFERENCES	52

TABLE OF FIGURES

Figure 1: Molecular mechanisms of autophagy.....	7
Figure 2: Two ubiquitin-like conjugation systems required for elongation of the autophagosomal membrane.....	9
Figure 3: Autophagic and apoptotic role of ATG12.....	12
Figure 4: ATG12 was co-localized with Mitotracker in HepG2 and MDA-MA-231 cells.....	30
Figure 5: ATG12 was co-localized with SSBP1 in HepG2 and CEM cells.....	31
Figure 6: ATG12 was not co-localized with LAMP1, ERAP1 and LC3 in MDA-MA-231 cells.....	32
Figure 7: Significant difference in co-localization between ATG12 and Mitotracker with ATG12 and LAMP1, ERAP1 and LC3 in MDA-MA-231 cells.....	33
Figure 8: ATG12 is present in the mitochondrial fraction.....	34
Figure 9: Mitochondrial localization of ATG12 is independent on Bcl-2 overexpression in CEM cells.....	37
Figure 10: Independency of ATG12 mitochondrial localization on Bcl-2 overexpression in CEM cells is shown with immunoblotting.....	38
Figure 11: Lower ATG12 expression in normal fibroblasts in comparison to liver cancer HepG2 cells.....	41
Figure 12: Significantly increased expression of ATG12 in colon, lung and mammary gland tumors tissues in comparison to their corresponding normal tissues.....	42
Figure 13: Significantly increased expression of ATG12 in prostate, esophagus and stomach tumors tissues in comparison to their corresponding normal tissues.....	43
Figure 14: Different molecular weights of ATG12-ATG5 conjugates detected with mATG12 and rATG12.....	45

ABSTRACT

Autophagy is a catabolic process by which cytoplasmic substrates are degraded through the formation of autophagosomes and their fusion with lysosomes. Autophagy is a protective mechanism against metabolic stresses, aging, infection, neurodegenerative diseases and cancer. Autophagic machinery is regulated by autophagy-related (ATG) genes, which were first discovered in yeast. To date, 19 mammalian homologues of yeast ATGs have been identified.

Several studies have indicated that autophagy plays a tumor suppressing role in the initiation phase of tumor formation and a tumor promoting role once the tumor has been established. This thesis seeks to further characterize autophagy-related protein 12 in human cancer cell lines. ATG12 as an ATG12-ATG5 conjugate is an essential protein in the elongation phase of autophagosome formation.

Using fluorescence microscopy and immunoblotting we were able to confirm the mitochondrial localization of ATG12, which had previously been revealed in our lab. Based on a recent study delineating an interaction between ATG12 and anti-apoptotic members of Bcl-2 family proteins, we had investigated whether Bcl-2 has an influence on ATG12 localization. We were able to determine that mitochondrial localization of ATG12 is Bcl-2 independent.

Further we have investigated expression of ATG12 in human tumor and normal tissues with tissue microarray. In tissues of 8 organs a significantly increased expression of ATG12 was seen in tumor tissues in comparison to their paired normal tissues.

Upon induction of autophagy the ATG12-ATG5 complex moves from cytosol to the growing autophagosomal membrane. Performing immunoblotting we detected the cytosolic and the mitochondrial ATG12-ATG5 complex. A slightly different molecular weight was observed between the two conjugates.

Our research contributes to a better understanding of the complex role of autophagy in cancer. Furthermore it indicates that autophagy-related proteins could play a role in tumorigenesis and might represent novel biomarkers and drug targets, respectively.

Key words: *autophagy, autophagy-related protein 12, Bcl-2, cancer*

RAZŠIRJENI POVZETEK

Avtofagija je kataboličen proces, ki igra pomembno vlogo pri ohranitvi celične homeostaze. S pomočjo avtofagije celice premagujejo različna stanja stresa, kot so pomanjkanje hranil, rastnih faktorjev in kisika, prekomerna prisotnost reaktivnih kisikovih spojin ter tudi okužbe s patogeni. Regulirana je z avtofagijo povezanimi (ATG) proteini, ki so bili prvotno odkriti v glivah kvasovkah. Do danes je bilo odkritih 19 sesalčevih homologov ATG proteinov.

Mehanizem avtofagije lahko razdelimo na tri dele. Z iniciacijo se začne formacija dvojne membrane, ki zajame tarčni del citoplazme. V fazi elongacije se dvojna membrana sklene in nastane za avtofagijo specifičen organel avtofagosom. V zadnji fazi, degradacijski, se avtofagosom združi z lizosomom in nastane avtofagolizosom. Zaradi hidrolizirajočih encimov, ki jih vsebuje lizosom, se razgradi zajeta citoplazemska vsebina avtofagosoma. Preko degradacijsko-regeneracijskega kroga, avtofagija konstantno zagotavlja pretok biomolekul, saj povzroča razgradnjo proteinov, lipidov, molekul DNA in RNA v osnovne molekule, ki se nato sprostijo v citoplazmo. Celice jih uporabijo za izgradnjo celičnih sestavin in produkcijo ATP. Poleg vzdrževanja energijske homeostaze, zagotavlja proces avtofagije tudi ustrezno kvaliteto proteinov in organelov prisotnih v celicah, tako da poškodovane ali odvečne razgrajuje. Na splošno avtofagija varuje organizem pred staranjem, rakom, nevrodegenerativnimi boleznimi in infekcijo.

Dosedanje študije so pokazale dvolično vlogo avtofagije v razvoju raka. V začetni fazi kancerogeneze se v procesu avtofagije odstranjujejo reaktivne kisikove spojine, poškodovani ali odvečni proteini in organeli. S tem se preprečuje njihovo nalaganje in zmanjšuje možnost razvoja rakavih celic. Z rastjo tumorja se zaradi pospešene rasti in nezadostne prekrvavitve rakavih celic ter terapijskih pristopov njihove potrebe po hranilih in kisiku povečujejo. Stanje stradanja in pomanjkanja kisika aktivira avtofagijo in ta deluje kot alternativen vir hranil in kisika ter tako pomaga rakavim celicam preživeti pod temi pogoji.

V magistrski nalogi smo se osredotočili na z avtofagijo povezanim proteinom 12 (ATG12). ATG12 v kompleksu z ATG5 (ATG12-ATG5) sodeluje pri podaljševanju dvoslojne membrane nastajajočega avtofagosoma in je eden izmed ključnih proteinov v elongacijski fazi avtofagije.

Namen magistrske naloge in eksperimentalni postopki

Namen raziskovalnega dela je bil čim boljše okarakterizirati ATG12. Sprva smo želeli potrditi hipotezo raziskovalne skupine, s katero sem sodelovala, o mitohondrijski lokalizaciji ATG12. Naš naslednji cilj je bil ugotoviti, ali je mitohondrijska lokalizacija ATG12 odvisna od izražanja Bcl-2. Nadalje smo z uporabo mikromreže, ki je vsebovala vzorce zdravega in rakavega tkiva organov, primerjali izražanje ATG12 med zdravim in rakavim tkivom. Posluževali smo se metod fluorescenčne mikroskopije in izvajali subcelularno frakcioniranje, kateri je sledila imunodetekcija proteinov po prenosu western.

Raziskovalno delo

S pomočjo fluorescenčne mikroskopije smo preverjali lokalizacijo ATG12 na mitohondriju v rakavih celicah jeter HepG2, celicah raka dojke MDA-MA-231 in T limfoblastoidnih celicah CEM. ATG12 in mitohondrije smo fluorescenčno označili z za njiju specifičnimi označevalci in opazovali celične preparate pod mikroskopom. Slike smo analizirali s pomočjo računalniškega programa, ki nam je izračunal Pearsonov koeficient korelacije (R), ki predstavlja stopnjo kolokalizacije preiskovanih proteinov. V vseh treh celičnih linijah smo dobili visoke R vrednosti, kar je nakazovalo na kolokalizacijo med ATG12 in mitohondriji. Da bi izključili možnost lokalizacije ATG12 na lizosomu ali endoplazmatskem retikulumu (ER), smo le-te fluorescenčno označili in opazovali njihovo morebitno kolokalizacijo. Iz nizkih vrednosti R, smo sklepali, da ATG12 najverjetneje ni lokaliziran na lizosomu ali ER. Postopek smo ponovili za preverjanje kolokalizacije med ATG12 in LC3. LC3 je z vezanim fosfatidiletanolaminom prisoten na notranji in zunanji membrani avtofagosoma in velja zato za specifičnega označevalca avtofagije. Nizka vrednost Pearsonovega koeficienta korelacije je nakazala zelo majhno kolokalizacijo med preiskovanima proteinoma.

Za dodatno potrdilo lokalizacije ATG12 na mitohondriju smo z rakavimi celicami jeter HepG2 izvedli subcelularno frakcioniranje, kjer smo ločili mitohondrijsko frakcijo od citosolne. Nato smo z imunodetekcijo proteinov po prenosu western ATG12 kot konjugat z ATG5 detektirali le v mitohondrijski frakciji, kar je potrdilo naše rezultate, pridobljene s fluorescenčno mikroskopijo o mitohondrijski lokalizaciji ATG12.

Odvisnost mitohondrijske lokalizacije ATG12 od izražanja Bcl-2, smo ugotavljali v celicah CEM s povečanim izražanjem antiapoptotičnega proteina Bcl-2.

Imunofluorescenčno smo označili ATG12 in mitohondrije ter primerjali R vrednosti kolokalizacije med opazovanima proteinoma. Vrednosti Pearsonovega koeficienta korelacije se med divjim tipom CEM in CEM s povečanim izražanjem Bcl-2 niso signifikantno razlikovale. Da bi preverili rezultate, pridobljene s fluorescenčno mikroskopijo, smo z obema celičnima linijama izvedli subcelularno frakcioniranje in s prenosom western smo zaznali ATG12 le v mitohondrijskih frakcijah. Intenziteta lis ATG12 se med celičnima tipoma ni razlikovala. Na podlagi rezultatov smo sklepali, da je mitohondrijska lokalizacija ATG12 neodvisna od izražanja Bcl-2.

Nadalje smo raziskovali, ali obstaja razlika v izražanju ATG12 med rakavim in zdravim tkivom. Zato smo uporabili tehnologijo mikromrež. Naš preparat je vseboval pare vzorcev zdravega in rakavega tkiva biopsij pacientov. S pomočjo imunohistokemije smo označili raziskovani protein in preparat opazovali pod mikroskopom. V kolonu, mlečnih žlezah, prostati, pljučih, skeletnih mišicah, požiralniku, modih in želodcu smo opazili signifikantno povišano izražanje ATG12 v rakavem tkivu v primerjavi z zdravim tkivom.

Ponovno smo izvedli subcelularno frakcioniranje rakavih celic pljuč H1299, dojke MDA-MA-231 in jeter HepG2 ter tako ločili mitohondrijsko frakcijo od citosolne. ATG12 smo tokrat detektirali z dvema različnima protitelesoma. Mišje ATG12 protitelo je tako kot prej detektiralo ATG12-ATG5 konjugat v mitohondrijski frakciji, zajče ATG12 protitelo pa ATG12-ATG5 kompleks v citosolu. Med ATG12-ATG5 konjugatom v citosolni in mitohondrijski frakciji smo opazili razliko v molekularni masi. Kot vemo, je ATG12-ATG5 kompleks lociran na citosolu in se med avtofagijo prenese na nastajajočo avtofagosomalno membrano. Glede na naše ugotovitve, da je ATG12-ATG5 kompleks lokaliziran tudi na mitohondriju, smo sklepali, da pod določenimi pogoji ATG12-ATG5 kompleks prehaja iz citosola na mitohondrij in da zaradi razlike v molekularni masi v določeni točki pride do postranslacijske modifikacije.

Naše raziskovalno delo je potrdilo kompleksno vlogo avtofagije pri rakavih boleznih in nakazalo pomembnost nadaljnjega raziskovanja avtofagije za pridobitev boljšega razumevanja njenega mehanizma. ATG12 in ostali proteini, ki regulirajo avtofagijo, bi lahko v prihodnost imeli vlogo tumorskih označevalcev v diagnozi in prognozi rakavih obolenj ter predstavljali nove tarče za zdravljenje raka.

Ključne besede: *avtofagija, z avtofagijo povezani protein 12, Bcl-2, rak*

LIST OF USED ABBREVIATIONS

ATG	Autophagy-related
BCA	Bicinchoninic acid
Bcl-2	B-cell lymphoma 2 protein
BSA	Bovine serum albumin
CQ	Chloroquine
DAPI	4',6-diamidino-2-phenylindole
DMSO	Dimethyl sulfoxide
DTT	Dithiothreitol
EBSS	Earle's Balanced Salt Solution
EDTA	Diaminoethane-tetraacetic acid
FCS	Fetal calf serum
HRP	horseradish peroxidase
mTOR	Mammalian target of rapamycin
NRF2	Nuclear factor erythroid-derived 2-like 2
PBS	Phosphate buffered saline
PFA	Paraformaldehyde
PGC-1 α	Peroxisome proliferator-activated receptor gamma coactivator 1-alpha
PI3K	Phosphoinositide 3-kinase
R	Pearson's correlation coefficient
SDS-PAGE	Sodium dodecyl sulfate polyacrylamide gel electrophoresis
TBS	Tris-buffered saline
TMA	Tissue microarray
ULK	Unc-51 like autophagy activating kinase

1 INTRODUCTION

1.1 Introduction to autophagy

The word autophagy was first used by Christian de Duve, a Nobel Prize-winning cytologist and biochemist, for his work on lysosomes. The word has Greek roots: “auto” means self and “phagy”, eating, so it literally means self-eating. Autophagy is a dynamic process in which cells form a double-membrane vesicle, whose expanding membrane encloses cytoplasmic cargo called autophagosome. After fusion with lysosomes, autophagosomes form autophagolysosomes, in which engulfed cytoplasmic substrates are degraded. This is a catabolic process in which unfolded or superfluous proteins and damaged organelles are recycled. Autophagy is constantly present at basal levels in almost all mammalian cells. Autophagy is involved in several mechanisms and pathways, including cell differentiation and development, aging, homeostasis, infection and immunity, quality control, neurodegeneration and cancer. Autophagy is regulated by genes called autophagy-related (ATG) genes, which were first discovered in yeast. To date, 37 ATG genes have been identified in yeast, including 19 mammalian homologues of yeast ATGs. There are three types of autophagy: microautophagy, chaperone-mediated autophagy and macroautophagy. This thesis focusses on macroautophagy, here referred to simply as autophagy (1, 2).

1.2 The physiological role of autophagy

Autophagy is a protective mechanism against metabolic stresses, such as nutrient deprivation, growth factor depletion and hypoxia. Cells have two mechanisms of intracellular protein degradation: the ubiquitin-proteasome system and the autophagy-lysosome system (1). During short periods of starvation the necessary amino acids are produced by the ubiquitin-proteasome system. If starvation is prolonged for hours, autophagy is the main mechanism that provides amino acids (3). In the last step of autophagy, degradation, autophagosomes fuse with lysosomes, which contain peptidases, lipases and nucleases. With the fusion and autophagolysosome formation, proteins, lipids, DNA and RNA are degraded into basic biomolecules, which are then released into the cytosol. Autophagy creates a flow of biomolecules in a degradation-regeneration cycle (4). With the degradation of cytoplasmic cargo, free amino and fatty acids are generated. These

can be further processed and used in the tricarboxylic acid cycle (TCA) for cellular ATP production (2).

Besides its function in energy homeostasis, autophagy also controls protein and organelle quality. Defective proteins and organelles (mitochondria, peroxisomes, endoplasmic reticulum [ER]) are degraded through autophagy, preventing their accumulation. Thus autophagy limits DNA damage and chromosomal instability (2, 5). Mitophagy, autophagic degradation of mitochondria, is the major pathway for mitochondria turnover. Mitophagy is induced by reactive oxygen species, which are produced by damaged mitochondria. Mitophagy malfunctioning could increase DNA damage, because of the accumulation of damaged mitochondria and free radicals, which increases the mutation rate and could eventually lead to diseases such as cancer and neurodegenerative disorders (6). Autophagy also fulfills a defense function against viral, bacterial and parasitic infections; it contributes to innate and adaptive immune activation (7). In sum, autophagy protects the organism against aging, cancer, neurodegenerative diseases and infection.

As described above, autophagy has an important role in cellular survival, but it is also considered to be a form of non-apoptotic programmed cell death (PCD), or autophagic cell death. Autophagosome formation increases in dying cells and autophagic features exist in regions where programmed cell death is occurring. Yet it remains difficult to determine whether autophagic activity in dying cells is a pro-survival mechanism or is the cause of death, as a form of PCD (2, 8).

1.3 Autophagy in cancer

The evidence indicates that autophagy has a tumor suppressing role in the initiation phase of tumor formation and a tumor promoting role once the tumor has been formed (9). Under normal conditions autophagy occurs at low basal level. It degrades unfolded proteins and damaged or superfluous organelles, thus preventing accumulation, and it controls organelle quality. In mice that were incapable of autophagy, accumulation of ubiquitinated protein aggregates, damaged organelles including mitochondria, peroxisomes, ER, ribosomes, and lipid drops were found. Consequently the absence of autophagy creates an imbalance in cellular homeostasis, a higher risk of tissue damage, and genome instability that could lead to tumor initiation (9, 10).

1.3.1 The role of autophagy in tumor suppression

The first evidence that linked autophagy to tumor suppression was the testing of mice with allelic loss of autophagy-related protein 6 (ATG 6), also known as Beclin 1 (Bcl-2-interacting protein-1). The mice were diagnosed with a high occurrence of tumors such as B cell lymphoma, hepatocellular carcinoma and lung adenocarcinoma (11). Allelic loss of Beclin 1 was also found in human breast, ovarian and prostate tumors. Beclin 1 was the first ATG that was defined as a tumor suppressor gene (10). The Beclin 1 binding protein UVRAG, a positive regulator of autophagy, suppresses the proliferation and tumorigenicity of human colon cancer cells (9). A mutation of Bax-binding protein 1 (Bif-1), also an inducer of autophagy, was found in colon adenocarcinomas (11). All these findings support the theory that autophagy is a tumor suppressor mechanism. How exactly autophagy suppresses tumorigenicity is still unclear, but there are several theories.

First, autophagy plays an important role in maintaining genome integrity. A study of mouse epithelial cells defective in autophagy (monoallelic loss of Beclin 1) and apoptosis (Bcl-2 overexpression) showed that these cells were more inclined to necrosis than cells with functional autophagy and also indicated a higher tumorigenic potential. A remarkable increase in DNA damage under metabolic stress was also found (11). In studies of mice that were incapable of autophagy, accumulation of p62, damaged organelles like mitochondria, ER, and elevated reactive oxygen species were also found. Normally, in intact autophagy, p62 levels are low, because it becomes degraded generally through autophagy. p62 activates nuclear factor erythroid-derived 2-like 2 (NRF2). The degradation of p62 and suppression of NRF2 is an important tumor suppressor mechanism (9). The main function of NRF2 is in suppressing oxidative stress, making it a major regulator of cell survival. It is known that activation of the NRF2 defense mechanism protects cells against several diseases including cancer, but the accumulation of NRF2 in cancer cells not only promotes cell survival in normal cells but also in cancer cells, protecting these against oxidative stress and chemotherapy. Consequently, p62 accumulates in cells with defective autophagy, so more NRF2 is activated (12). Altogether, cells with defective autophagy have a higher risk of tissue damage and genome instability, which could lead to tumor initiation, while accumulation of p62 could also lead to cancer progression (9, 10).

Another way in which autophagy mediates tumor suppression is by limiting the ability of tumor cells to undergo necrosis. Apoptosis-defective cells with impaired autophagy are more likely than cells with unimpaired autophagy to undergo necrotic cell death under conditions of metabolic stress. Hypoxia and metabolic stress commonly affect solid tumors. Necrotic cell death results in an inflammatory response with infiltration of pro-tumor inflammatory mediators. Infiltration correlates with enhanced tumor growth and poor clinical prognosis. Autophagy acts as a tumor suppressor by limiting necrotic cell death and metabolic stress (11, 13).

Autophagy also acts as a tumor suppressor by mediating oncogene-induced senescence (OIS). Senescence represents an irreversible cell cycle arrest with metabolically viable cells. It limits the proliferation of abnormal cells and is thus an early barrier to cancer development. As the name suggests, it is activated by oncogenes, such as RAS, as a response to their hyperproliferation signals. The RNAi knockdown of ATG5 or ATG7 makes it easier for cells to bypass OIS, while the induction of autophagy enhances senescence-associated cytokine production. This indicates that autophagy is an important factor in the establishment of OIS, and is thus capable of limiting the accumulation of genomic alterations and tumor progression (11, 14, 15).

1.3.2 The role of autophagy in tumor progression

The first indication that autophagy could play a role in promoting tumorigenesis was the discovery that autophagosomes in cancer cells were mostly located in tumor hypoxic areas and that autophagy inhibition caused tumor cell death in these regions in particular (10).

With tumor growth, tumor cells are under metabolic stress, due to the high metabolic demands on nutrients and oxygen ensuing from their high proliferation rate, insufficient vascularisation and therapeutic approaches (1). Starvation and hypoxia activate autophagy in the less vascularised areas of primary tumors. It acts as an alternative source of energy and protects cells against necrosis and apoptosis, helping tumor cells to survive under these conditions, and therefore plays a crucial role in cancer progression (11, 14).

Another crucial step in which autophagy plays an important role is metastasis. Tumor cells need to activate mechanisms that assist them in overcoming the stress of extracellular matrix (ECM) detachment, otherwise this could lead to anoikis. Anoikis is a form of

programmed cell death which is induced by the detachment of cells from the ECM. Cancer cell resistance to anoikis is a crucial step in tumor progression and metastatic colonisation. It is a protective mechanism that prevents cell growth and colonisation on an improper matrix and in distal organs. Autophagy is activated by detachment from the ECM and protects cells against anoikis, through which it promotes metastasis (11, 14, 16).

Furthermore, it was reported that autophagy could contribute to tumor cell resistance to anti-cancer therapy (1). Most chemotherapeutic agents create stress conditions which cancer cells have to overcome in order to survive. The activation of autophagy by stress conditions could be a survival mechanism for cancer cells to resist chemotherapy (17). Several studies have confirmed autophagy as a protective mechanism against chemotherapy. In studies of 3-MA (3-Methyladenine) inhibited autophagy in human colorectal cancer cells, the cytotoxicity of 5-fluorouracil was enhanced (14). Additionally, a delay in melanoma cell death was reported in melanoma treatment with esomeprazole in combination with the induction of autophagy. Moreover esomeprazole efficiency as a chemotherapeutic drug against melanoma was increased with knocking down ATG5 or Beclin 1 expression (9).

It is clear that autophagy plays an important and very complex role in tumorigenesis and resistance to cancer therapy. Therefore a better understanding of autophagy machinery in cancer is of great significance and merits further investigation.

1.4 Molecular mechanisms of autophagy

The molecular mechanism of autophagy may be divided in to 4 main steps: initiation, autophagosome formation, fusion of autophagosomes with lysosomes and degradation. Autophagic machinery is regulated by autophagy-related (ATG) proteins. The process of autophagy begins by the formation of an isolation membrane or phagophore, the exact origin of which is still unclear. The phagophore membrane is derived from a lipid bilayer which most probably originates from ER and/or Golgi and endosomes (18, 19, 20).

The initiation phase is regulated by mammalian target of rapamycin (mTOR) and by two kinases, class I and class III phosphoinositide 3-kinase (PI3K). Autophagy is initiated by activation of the ULK1/2 complex, which is regulated by mTOR. In the presence of nutrients, growth factors and oxygen mTOR is activated with class I PI3K and suppresses

autophagy by binding to the ULK1/2 complex. In nutrient poor conditions mTOR is inactive and it dissociates from the ULK1/2 complex, thus allowing the ULK1/2 complex to accumulate at the isolation membrane, also called the phagophore. There, ULK1/2 regulates the traffic of ATG9, which is probably responsible for the supply from donor sources to the phagophore of lipids necessary for membrane elongation and nucleation. ULK1/2 is also responsible for the proper localization of the class III PI3K complex at the phagophore, where it generates phosphatidylinositol 3-phosphate (PI3P), which recruits other ATG proteins necessary for the expansion of the phagophore to form a double-membrane vesicle, the autophagosome (4, 18, 21).

Two ubiquitin-like conjugation systems are implicated in the completion of the autophagosome. The first includes formation of the multimeric complex ATG12-ATG5-ATG16L, which is necessary for the elongation of the autophagosomal membrane and may play a role in autophagosome curvature. The second ubiquitin-like conjugation system involves the transformation of LC3 into LC3-PE. LC3 is first cleaved to LC3-I and then conjugated with phosphatidylethanolamine (PE) to form LC3-II or LC3-PE. ATG12-ATG5-ATG16L acts as an E3 ligase in LC3-PE conjugation and is responsible for the recruitment of LC3-II to the phagophore. LC3-II is symmetrically bound to the inner and outer autophagosomal membrane (22, 23, 24). The LC3-II on the inner membrane is degraded by the autophagosomal machinery and LC3-II on the outer membrane is cleaved by ATG4 and recycled. The lipidated LC3-PE is specifically localized on the autophagosomal membrane and the level of LC3-PE also correlates with autophagosome numbers, so it is a specific marker for autophagy (4, 20). It has been reported that in yeast, lower levels of LC3 proteins reduced the size of autophagosomes, but this did not affect their number (25).

In the final degradation step, mature autophagosomes fuse with lysosomes to form autolysosomes. The outer autophagosomal membrane fuses with lysosomes and the inner membrane is degraded together with its cargo of lysosomal hydrolases and lipases (4, 24, 26).

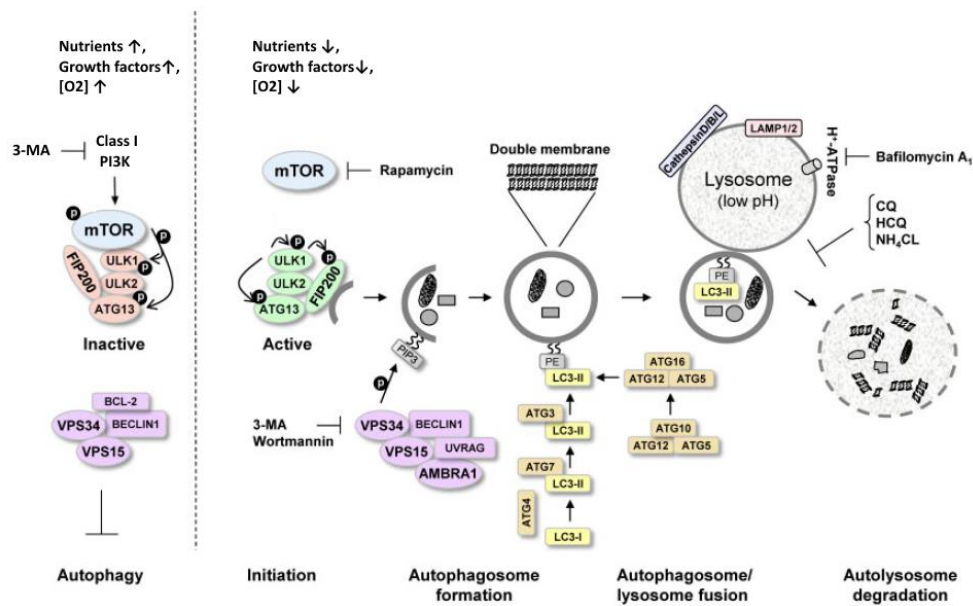


Figure 1: Molecular mechanisms of autophagy. The ULK1/2 complex consists of ULK1, ULK2, ATG13 and FIP200. After mTOR is activated by class I PI3K it suppresses autophagy by binding and phosphorylating ULK1/2 and hyperphosphorylating ATG13, thus inhibiting the serine/threonine kinase activity of ULK1. Under nutrient poor conditions or with rapamycin treatment, mTOR is inactive and it dissociates from the ULK1/2 complex. Activated ULK1 is autophosphorylated and phosphorylates ATG13 and FIP200, the complex relocates to the phagophore membrane, and autophagy is initiated. Activated ULK1 also phosphorylates AMBRA1, which binds both the microtubule-based molecular dynein motor complex and the class III PI3K complex (class III PI3K/VPS34, VPS15, Beclin 1, AMBRA 1, ATG14L). Phosphorylated AMBRA1 is released from the dynein complex and is translocated to the phagophore membrane together with class III PI3K complex. Bcl-2 inhibits autophagy, thus it interacts with the class III PI3K complex through Beclin 1. Additional proteins also interact with the class III PI3K complex, such as Bif-1, which directly interacts with UVRAG and acts as a positive autophagy regulator. Rubicon also interacts with Beclin 1, but acts as a negative regulator. Autophagosome completion is mediated by ATG12-ATG5-ATG16L and the LC3-PE conjugation systems. In the fusion machinery of autophagosomes with lysosomes reportedly LAMP1/2 (lysosome proteins) and cathepsin D/B/L are involved. Several pharmacological inhibitors can be used as activators or inhibitors of autophagy. The mTOR inhibitor rapamycin promotes induction of autophagy. 3-MA is a class I and class III PI3K inhibitor and Wortmannin is a class III PI3K inhibitor, thus they inhibit autophagy at early stages. Bafilomycin A, chloroquine, hydrochloroquine and NH_4Cl prevent the fusion of autophagosomes and lysosomes (26, 27, adapted from 27).

Several pharmacological inhibitors can disrupt the autophagic process at different stages and these are used in research into the role of autophagy in tumorigenesis. 3-Methyladenine (3-MA) is a class I and class III PI3K inhibitor. It inhibits autophagy at the initiation phase by inhibiting the formation of autophagosomes (28). Chloroquine (CQ) has

been used extensively in the treatment of malaria and it inhibits autophagy at the degradation phase. CQ accumulates inside lysosomes, and as it is a weak base it raises the lysosomal pH, which leads to the inhibition of lysosomal enzymes and prevents the fusion of lysosomes and autophagosomes. Due to its role in autophagy, it has also been studied as a potential agent in cancer therapy (29, 30). Bafilomycin A is a macrolide antibiotic whose action affects the degradation phase in the same way as chloroquines. It disrupts the proton gradient through inhibiting H⁺ ATPase, which raises the lysosomal pH (31). In contrast to the drugs mentioned above, rapamycin induces autophagy by binding to and inactivating mTOR. Rapamycin possesses immunosuppressive properties and is used in organ transplants (32).

1.5 Interaction factors of Autophagy-related protein 12

1.5.1 Autophagy-related protein 12

ATG12 is an ubiquitin-like protein of 140 amino acids (33). With western blotting of ATG12 two bands are observed, one at 17 kDa which belongs to single ATG12 and a higher band at 55 kDa that belongs to the ATG12-ATG5 conjugate. As mentioned above, ATG12 is part of the first ubiquitin-like conjugation system required in the elongation phase of autophagy. First ATG12 is activated by the E1-like enzyme ATG7, then ATG12 is directly transferred to the E2-like enzyme ATG10, forming a thioester. Finally ATG12 is transferred and covalently attached to ATG5, forming an isopeptide. The ATG12-ATG5 conjugate also forms a multimeric complex with ATG16L, which is responsible for recruiting the conjugate from cytosol mainly to the outer surface of the growing autophagosomal membrane. The multimeric complex is required for the expansion and closure of the autophagosomal membrane. It also acts as an E3 ligase in LC3 lipidation, where it transfers LC3-I from ATG3 to PE (34, 35, 36).

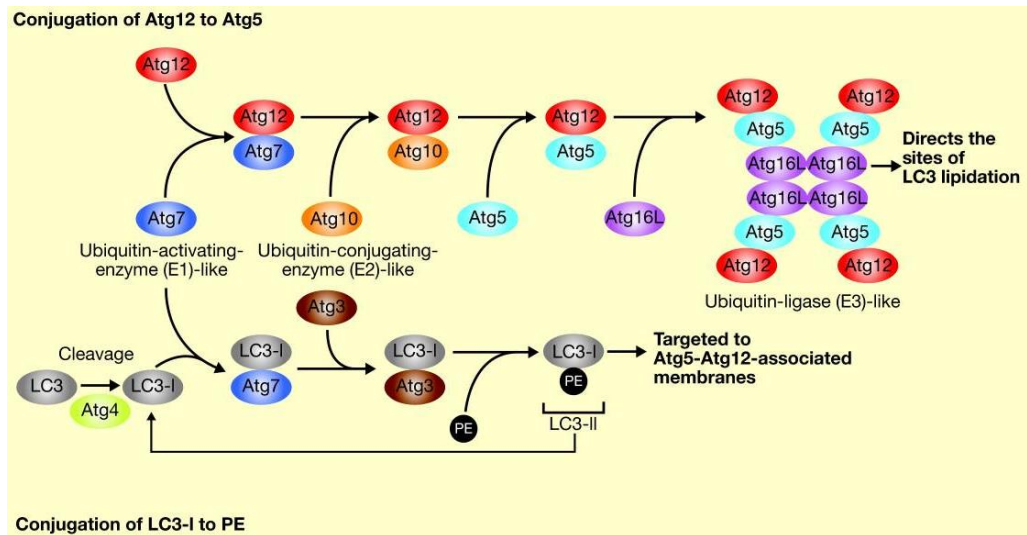


Figure 2: Two ubiquitin-like conjugation systems required for elongation of the autophagosomal membrane. The conjugation of ATG12 to ATG5 involving the E1-like enzyme ATG7 and E2-like enzyme ATG10 is shown above. ATG12-ATG5 conjugate also forms a multimeric complex with ATG16L due to ATG16L self-oligomerisation. The conjugation of LC3 to LC3-PE is shown below. LC3 is cleaved by ATG4 into LC3-I, which is then activated by the E1-like enzyme ATG7 and transferred to the E2-like enzyme ATG3, before becoming conjugated through an amide bond with a membrane lipid phosphatidylethanolamine (PE) to form LC3-II (36).

1.5.2 B-cell lymphoma 2 protein (Bcl-2)

1.5.2.1 The Bcl-2 family proteins

Apoptosis, also called programmed cell death, plays a crucial role in physiological and pathological conditions. One of the key stages in cancer development and progression is cancer cells gaining the ability to suppress apoptosis. Apoptosis is triggered through two main pathways, the intrinsic, which targets mitochondria functionally and the extrinsic, or death receptor pathway. An additional pathway is known as the intrinsic endoplasmic reticulum pathway. Each pathway is activated by specific triggering signals. The intrinsic and extrinsic pathways each activate their own initiator caspases, which in turn come together in the execution pathway by activating caspase 3, also called execution caspase. This then eventually leads to morphological changes and cell death. The intrinsic path is triggered by internal stimuli such as DNA damage, high concentrations of cytosolic calcium, hypoxia, oxidative stress, and radiation. It results in higher mitochondria

permeability and the release of two pro-apoptotic protein groups, including cytochrome C, into the cytosol (37, 38).

These apoptotic mitochondrial events are regulated by Bcl-2 family proteins. So far 25 proteins of the Bcl-2 family have been identified. These can be divided into three groups, pro-apoptotic (including Bax, Bad, Bak, and Bok), anti-apoptotic (including Bcl-2, Bcl-xL, Bcl-w, and Mcl-1) and BH3-only proteins (including Bim, Bid, and Bad).

All of the Bcl-2 family members contain at least one of four Bcl-2 homology (BH) domains; BH1, BH2, BH3, BH4. Bcl-2, Bcl-w and Bcl-xL conserve all four domains, whereas some Bcl-2 proteins have only the BH3 domain; these are called the BH3-only proteins. All pro-apoptotic members contain the BH3 domain, which is required for their pro-death activity. The BH3 domain contains a α -helical structure that enables binding to the hydrophobic groove of anti-apoptotic Bcl-2 family proteins (39, 40, 41).

Whether apoptotic cell death will be initiated or aborted depends on the balance of pro and anti-apoptotic Bcl-2 family proteins. The main mechanism of the Bcl-2 family is to regulate mitochondria permeability (37, 38).

Pro-apoptotic members of the Bcl-2 family are found mainly on the cytosol and are relocated after activation to the mitochondria membrane, which triggers mitochondrial outer membrane permeabilization (MOMP). Anti-apoptotic proteins prevent MOMP by inhibiting the activation of pro-apoptotic proteins due to their ability to bind to the BH3 region of pro-apoptotic proteins, therefore preventing the release of cytochrome C from mitochondria (39, 40, 41).

1.5.2.2 Interaction of ATG12 with Bcl-2

The molecular crosstalk between apoptosis and autophagy is complex and very poorly understood. For example Bcl-2 family proteins regulate both autophagy and the intrinsic apoptotic pathway. Bcl-2 and Bcl-2 related proteins bind to Beclin 1, inhibiting autophagy, whereas the pro-apoptotic BH3-only proteins disrupt the interaction between Bcl-2 and Beclin 1, promoting autophagy. Furthermore, as described below, caspase 3 is activated in apoptosis and also inhibits autophagy by cleaving Beclin 1.

A recent study determined another protein involved in the crosstalk between autophagy and apoptosis, which is ATG12 (42). An interaction between ATG12 and members of the

Bcl-2 family was observed and ATG12 was identified as a pro-apoptotic protein. The initial aim was to determine which ATG acts as a positive modulator of apoptosis by knocking down different ATG genes using siRNAs. Different cell types were then exposed to several apoptosis triggers and the range of apoptosis was defined with the activity of caspase 3 and caspase 7. The most significant difference in comparison to the control cells was with knockdown ATG12 cells, which led to notable caspase inhibition. Therefore it was suggested that ATG12 acts as a positive mediator of apoptosis.

Furthermore, a BH3-like region was detected in ATG12 with similar sequence to that in BH3-only proteins. Like the BH3-only proteins, ATG12 contains only the BH3-like domain. It was demonstrated that ATG12 interacts with Bcl-2 and Mcl-1, which requires the BH3-like region in ATG12 as well as the hydrophobic groove of the anti-apoptotic proteins. It was also investigated whether conjugation of ATG12 to its other interaction partners, ATG5 and ATG3, was needed for its binding to Bcl-2. The interaction of ATG12 with Bcl-2 was compared in wild type cells and in cells incapable of conjugating to ATG5 or ATG3. No difference in binding efficiency was seen, thus it was shown that unconjugated ATG12 is sufficient for binding Bcl-2. It was also investigated whether ATG12 induces apoptosis in a similar way to BH3-only proteins. The ability of ATG12 to induce apoptosis was shown to depend on binding anti-apoptotic Bcl-2 family proteins. The suppression efficiency of ATG12 was also unaffected by conjugation to ATG5 or ATG3. Furthermore, the depletion of ATG12 in apoptotic cells blocked pro-apoptotic protein Bax activation, leading to significantly reduced release of cytochrome C from mitochondria. In addition it was reported that mutation in the BH3-like region of ATG12 had no effect on autophagy (42, 43).

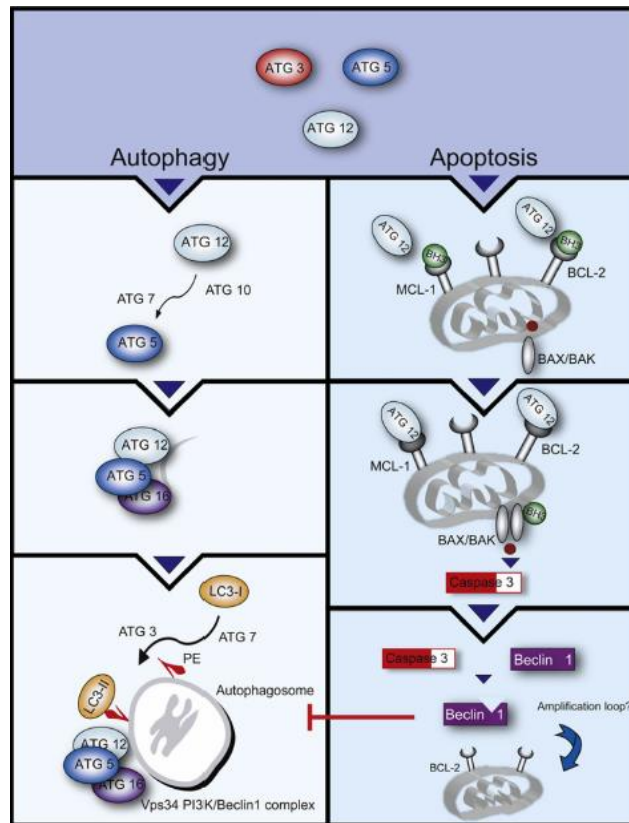


Figure 3: Autophagic and apoptotic role of ATG12. The autophagic pathway is shown on the left. Two ubiquitin-like conjugation systems (ATG12-ATG5-ATG16L complex and LC3-II) are formed, leading to autophagosome formation. The apoptosis pathway is shown on the right. After pro-apoptotic proteins Bax or Bak are activated, they undergo conformational changes and are relocated from cytosol to the outer mitochondrial membrane, where they form a channel through which cytochrome C and other pro-apoptotic proteins are released. As mentioned above, this leads to caspase 3 activation. ATG12 contains a BH3-like region, through which it binds to Mcl-1 and Bcl-2 and, similarly to pro-apoptotic Bcl-2 members, promotes apoptosis. After caspase 3 is activated, Beclin 1 is cleaved into three fragments. The Beclin 1-C fragment demonstrates an apoptosis-promoting function through encouraging the release of pro-apoptotic proteins from mitochondria. Cleaved Beclin 1 is incapable of activating the autophagic pathway (42, 43).

1.5.3 Autophagy-related protein 3

Another interactional factor of ATG12 that has been identified so far is ATG3. As mentioned above, ATG3 is part of an ubiquitin-like protein system required for autophagosome formation. ATG3 acts as an E2-like enzyme and mediates the conjugation of LC3 with PE.

The formation of ATG12-ATG3 complex is similar to that of ATG12-ATG5. First ATG12 is activated with the E1-like enzyme ATG7. ATG3 then acts as an E2-like enzyme and covalently binds to ATG12 (28). In contrast with ATG5, which appears only in conjugation with ATG12, free ATG3 is present concomitantly with ATG12-ATG3 in mammalian cells. Disruption of the ATG12-ATG3 complex has no influence on lipidation of LC3-I or on nonselective autophagy. It does however lead to the dysregulation of mitochondria homeostasis with an increase in mitochondrial mass and resistance to mitochondria mediated apoptosis. Cells with mutated ATG3 (ATG3KR - unable to conjugate with ATG12) showed a significant reduction in mitophagy in comparison to wild type ATG3 (WT-ATG3) cells upon mitochondria depolarisation (44). This suggests that the ATG12-ATG3 complex plays a role in targeting mitochondria to autophagosomes. Furthermore, cells with a mutant version of ATG3 showed fragmentation in the mitochondria network. The correct balance between mitochondrial fusion and fission is important for maintaining mitochondrial function and structure. Cells with ATG3KR showed dysfunction in mitochondria fusion machinery. Additionally, ATG3KR cells were less sensitive to mitochondria mediated apoptosis, and resistance to mitochondria cell death in ATG3KR cells correlates well with an increase in basal levels of Bcl-X_L, which is one of the anti-apoptotic Bcl-2 proteins (44, 45). The exact mechanism of ATG12-ATG3 regulation of mitochondria homeostasis is still unclear. The role of the ATG12-ATG3 complex in mitochondria homeostasis, mitophagy and the intrinsic apoptotic pathway makes it a significant subject for future investigation.

1.5.4 Autophagy-related protein 5

ATG5 was the first known interaction partner of ATG12 and is one of the key proteins in regulating autophagy. Its significance has made it the subject of several studies. Recent research on melanoma cells found reduction of ATG5 expression in primary melanomas in comparison to benign nevi. Furthermore, the reduction in LC3 expression correlated well with down-regulation of ATG5 expression, and the increased level of p62, a protein that is degraded through autophagy, was significantly higher in melanoma patients than in those with benign nevi. These findings indicate a reduction in autophagy as a result of down-regulation of ATG5 expression. Progression free survival was better in melanoma patients with higher ATG5 expression. Interestingly, in comparison to primary melanomas, ATG5

expression was normal in metastatic melanomas (46). The importance of ATG5 was also shown in ATG5-deficient mice, which died within 24 hours of delivery (47).

In a recent study, Jurkat T cells were treated with a sublethal concentration of DNA-damaging agents, such as etoposide or cisplatin. After four days of treatment, induction of autophagy with increased ATG5 expression was observed. ATG5 was mostly seen as the ATG12-ATG5 conjugate and also as an ATG5 monomer. Induction of autophagy as a result of treatment with anti-cancer drugs could contribute to the resistance of cancer cells to anti-cancer treatment (48).

2 OBJECTIVES

This research work is based on previous findings of host research group. Preliminary results indicated mitochondrial localization of ATG12. Induction of autophagy with starvation media, led to decreased levels of ATG12. Down regulation of ATG12 resulted in reduced number of mitochondria when compared to control cells.

The aim of presented thesis was to further characterize autophagy-related protein 12. First, we want to confirm mitochondrial localization of ATG12. Our second goal is to determine whether mitochondrial localization of ATG12 is Bcl-2 dependent. Furthermore, we want to compare the relative expression of ATG12 in tumor tissues to normal tissues using tissue microarrays. The main methods used are immunoblotting and immunofluorescence staining.

3 MATERIALS AND METHODS

3.1 Materials

Table I: Equipment

Name	Type	Company
Fume hood		Thermo Fisher Scientific
Incubator	Heraeus HERAcell 150i	Thermo Fisher Scientific
Incubator	Heating block DB-2D Dri-Block	Techno
Centrifuge	Heraeus Multifuge 3SR	Thermo Fisher Scientific
Centrifuge	Heraeus Megafuge 40R	Thermo Fisher Scientific
Microcentrifuge	Centrifuge 5417	Eppendorf
Microcentrifuge	Centrifuge 5417 R	Eppendorf
Cytocentrifuge	Shandon CytoSpin 3	Thermo Scientific
Vortex mixer	Vortex-Genie 2	Scientific Industries
Electrophoresis machine	Powerpac 3000	BioRad
Electrophoresis System	XCell SureLoc Mini-Cell	Life Technologies
Autoradiography film	Amersham Hyperfilm ECL	GE Healthcare
Transfer membrane	Immobilon – P	EMD Millipore
Counting chamber	Neubauer Improved	Assistent
Electronic balance	PM4000	Mettler Toledo
Electronic analytical balance	XP205	Mettler Toledo
Microplate reader	SpectraMax M2	Molecular devices
Imaging System	X-Omat 2000 processor	Kodak
Light microscope (inverted fluorescent)	Zeiss Axiovert 35	Carl Zeiss
Confocal microscope	LSM 5 Exciter	Carl Zeiss
Freezer (-20 °C)	G 3513	Liebherr
Freezer (-80 °C)	MDF-5386SC	Sanyo
Cryogenic vial	Nunc CryoTubes; 1.8 ml	Sigma
Falcon tubes	PP tubes with screw cup; 15 ml, 50 ml	Greiner Bio-One
Cell culture plates	6-, 24- and 96-well plates	Greiner Bio-One
Cell culture flasks	TC Flasks with filter cap; 50 ml, 250 ml, 550 ml	Greiner Bio-One

Pipettes	2.5 µl, 10 µl, 100 µl, 1000 µl	Eppendorf
Micro Test Tube	3810X; 1.5 ml	Eppendorf
Serological pipette	5 ml, 10 ml, 25 ml	Eppendorf
Aspirating pipette	2 ml	Greiner Bio-One
Cryogenic vial	Nunc CryoTubes; 1.8 ml	Sigma
Pipette boy	Pipettboy acu	INTEGRA Biosciences
Oven	Modell 500	Memmert

Table II: Chemicals

Name	Company
DMEM + GlutaMAX (Dulbecco's Modified Eagle Medium)	Invitrogen, Life Technologies
RPMI medium 1640 + GlutaMAX	Invitrogen, Life Technologies
FCS (Fetal calf serum)	PAA Laboratories
PBS	PAA Laboratories
Trypsin – EDTA	Life Technologies
Protease inhibitor cocktail (104 mM AEBSF, 80 µM Aprotinin, 4 mM Bestatin, 1.4 mM E-64, 2 mM Leupeptin, 1.5 mM Pepstatin A)	Sigma
Novex Sharp Pre-Stained Protein Standard	Invitrogen, Life Technologies
RunBlue 12% SDS PAGE Precast Gel	Expedeon
Restore Western Blot Stripping Buffer	Thermo Scientific
Pierce BCA Protein Assay Kit	Thermo Scientific
Pierce ECL Plus Western Blotting Substrate	Thermo Scientific
Amersham ECL Prime Western Blotting Detection Reagent	GE Healthcare
Luminata Forte Western HRP substrate	EMD Millipore
NuPAGE LDS Sample Buffer (4X)	Invitrogen, Life Technologies
RunBlue SDS Running buffer (20X)	Expedeon
EBSS	Life Technologies
Chloroquine	Sigma
BSA Fraction V Solution (7.5%)	Life Technologies
ProLong Gold Antifade Reagent with DAPI	Life Technologies
Mitotracker Orange (CMTMRos)	Molecular probes
Mouse ATG12 Antibody	R&D Systems

Rabbit ATG12 Antibody	Cell Signaling Technology
Mouse ATG5 (7C6) Antibody	NanoTool
Mouse ATG5 (11C3) Antibody	NanoTool
Mouse GAPDH Antibody	EMD Millipore
Rabbit LC3 Antibody	Cell Signaling Technology
Mouse MTC02 Antibody	Abcam
Rabbit LAMP-1 Antibody	Abcam
Rabbit ERAP-1 Antibody	Abcam
Rabbit SSBP-1 Antibody	Novus Biologicals
Mouse Bcl-2 Antibody	Zymed
Secondary fluorescent mouse Antibody from goat	LI-COR Biosciences
Secondary fluorescent rabbit Antibody from goat	LI-COR Biosciences
Antimouse IgG, HRP-linked whole Antibody from sheep	GE Healthcare
ECL Rabbit IgG, HRP-linked whole Antibody from donkey	GE Healthcare
Goat-anti-mouse Antibody, 555	Invitrogen, Molecular probes
Goat-anti-mouse Antibody, 488	Invitrogen, Molecular probes
Goat-anti-rabbit Antibody, 488	Invitrogen, Molecular probes
DAKO target retrieval solution 1x	DAKO
DAKO dual endogenous enzyme block	DAKO
DAKO antibody diluent	DAKO
DAKO biotinylated secondary antibody	DAKO
DAKO strepdavidin alkaline phosphatase	DAKO
Hematoxylin	Sigma-Aldrich

Table III: Prepared solutions

Name	Components
TBS (10X)	0.20 M Tris, 1.50 M NaCl [pH=7.6]
TBST	0.1% Tween 20 in TBS
Transfer buffer (10X)	0.25 M Tris, 1.87 M Glycine
Transfer buffer	20% MeOH in 1X Transfer buffer
Running buffer 20X	5% Running buffer
Blocking buffer for western blot	5% milk powder in TBST

Blocking buffer for immunofluorescent staining	3% goat serum and 1:200 of 10% saponin in PBS
Cytosolic extraction buffer (CEB)	20 mM HEPES [pH 7.2], 250 mM Sucrose, 10 mM KCl, 1.5 mM MgCl ₂ , 2 mM EDTA
Complete cytosolic extraction buffer (CCEB)	CEB with 100 μM PMSF, 1 mM DTT, 0.1% protease inhibitor cocktail
Lysis buffer	50 mM Tris [pH 7.4], 150 mM NaCl, 10% Glycerol, 1% Triton X-100, 2 mM EDTA, 10 mM NaPyrophosphate, 50 mM NaF, 200 μM Na ₃ VO ₄
Substrate working solution	750 μl AP substrate buffer with levamisole (1:1000 levamisole in AP substrate buffer), 30 μl Chromogen RED 1, 30 μl Chromogen RED 2, 30 μl Chromogen RED 3

3.2 Methods

3.2.1 Cell culture

Five cell lines were used to further characterize autophagy-related protein 12.

Table IV: Cell lines used for experiments

Cell type	Tissue type	Media	Growing type
MDA-MA-231	Breast	DMEM + GlutaMAX (Dulbecco's Modified Eagle Medium)	Adherent
HepG2	Liver	DMEM + GlutaMAX (Dulbecco's Modified Eagle Medium)	Adherent
H1299	Lung	RPMI medium 1640 + GlutaMAX	Adherent
CEM	T lymphoblastoid	RPMI medium 1640 + GlutaMAX	Suspension
Fibroblast	Skin	DMEM + GlutaMAX (Dulbecco's Modified Eagle Medium)	Adherent

3.2.1.1 Cell passaging

Cell passaging involves splitting cells and transferring them into new flasks. Ideally, cells should be passaged during the late log phase of cell growth, a period where cells proliferate exponentially. All of the cells may be used and expanded for any sort of experiment or only some of them may be used for culture and the rest discarded.

Adherent cells are kept in their corresponding culture media (Table IV) which contains 10% FCS and 1% P/S (10000 units/ml of penicillin and 10000 µg/ml of streptomycin) in the incubator at 37 °C with 5% CO₂.

First the media is removed using a vacuum pump and the cells are washed with PBS (Phosphate Buffered Saline). Then 0.5 ml (for a small flask), 1 ml (for a middle flask), or 2 ml (for a big flask) of Trypsin EDTA is added to the flask and equally distributed over the cell area. Then the flasks are incubated for 5 min at 37°C to detach the cells.

The cells are resuspended by adding 4.5 ml (for a small flask), 9 ml (for a middle flask), or 18 ml (for a big flask) of their corresponding culture media. Cells need to be well mixed by pipetting up and down until no cell clusters are seen. The appropriate amount of cells is then transferred to one or more new flasks, which already contain fresh culture media. The cells are then kept in the incubator for a new growing phase.

Passaging suspension cell lines is less complicated, because they are not attached to the surface. Therefore the appropriate amount of cells can be directly transferred to new flasks and appropriate amount of culture media added. These can be left in the flask and fed every 2 to 3 days by adding fresh culture media until they reach confluency.

3.2.1.2 Cell freezing

First cells are detached from the culture flask and resuspended in culture media. Then they are transferred to a 15 ml falcon tube. They are centrifuged at 1400 rpm for 5 min at room temperature. The supernatant is carefully removed with a vacuum pump. The cell pellet is resuspended with 900 µl of FCS and transferred to the cryotube. Then 100 µl of DMSO is added and the cells are mixed well with the pipette to form a homogenous suspension. The tube is closed and stored at -80 °C overnight. Then the cryotubes are transferred to liquid nitrogen for undetermined storage.

3.2.1.3 Cell thawing

Cryotubes containing cells are transferred from liquid nitrogen to a 37°C water bath in order to thaw the cells more rapidly. 1 ml of cells is then transferred to a 15 ml falcon tube which contains 9 ml of culture media. The cells are centrifuged at 1400 rpm for 5 min at room temperature. The supernatant is carefully removed with a vacuum pump. Cells are

resuspended with 1 ml of fresh culture media and are then transferred to a new flask, filed with fresh media. The cells are incubated at 37 °C with 5% CO₂ for culture.

3.2.2 Measuring protein concentrations

The protein concentrations are determined using a Pierce BCA protein assay kit with a SpectraMax M2 machine at 540 nm.

Lysed samples and eight BCA standard solutions are taken from -20 °C and put on ice to thaw. Lysed samples are centrifuged at 13300 rpm for 10 min at 4 °C. The supernatant is transferred to a new Eppendorf tube and is used for protein measurements. Meanwhile a mixture of BCA reagent A and B is prepared in the ratio 50:1. Before measurement the lysed samples need to be diluted at a ratio of 1:10.

For protein measurement a 96-well plate is used. First 25 µl of prepared BCA standard solution and diluted lysed sample are pipetted into the wells of a 96-well plate, each in duplicate. Then 200 µl of mixed BCA reagent A and B is added to each filled well. The plate is incubated at 37 °C for 5 min. Then the protein concentrations are measured with the SpectraMax M2 machine at 540 nm.

3.2.3 Western blotting

After measuring protein concentrations, the appropriate amount of lysate, distilled water, loading buffer (4x) and DTT (10x) are calculated and added to new Eppendorf tubes. Loading buffer is diluted at a ratio of 1:4 and DTT at 1:10. The usual amount of loaded proteins is between 30-50 µg per sample and the loading volume is normally between 20-30 µl. The prepared samples are boiled at 90 °C for 5 min to denature proteins. After the samples are cooled they are centrifuged at 13000 rpm for 3 min.

Next, the chamber for electrophoresis is prepared by inserting one or two of 12% SDS-PAGE gels and filling it with 800 ml of running buffer (Table III), which is diluted at a ratio of 1:20. The gel wells are washed with the running buffer by pipetting up and down. One gel contains 12 wells. First the molecular weight markers are loaded, then an equal amount of proteins are put into the wells. The chamber is closed and the electrophoresis can begin. The gel runs for 30 min at 80 V, followed by 1 h at 135 V. The electrophoresis stops when the blue markers reach the end of the gel.

Meanwhile the transfer buffer (Table III) needs to be cooled down at 4 °C together with the cassette holder, 5 or 6 sponges, 2 filters, Whatman papers and a polyvinylidene difluoride (PVDF) membrane. In order to run one gel, one PVDF membrane and two Whatman papers are needed, to run two gels, two PVDF membranes and four Whatman papers are needed. Most importantly at this stage, the membrane needs to be labelled and activated by rinsing it in methanol for 1 min, before putting it in the transfer buffer. When the electrophoresis is finished, the gel is removed from the chamber. The transfer stack is prepared by first putting 2 or 3 sponges on the back side of the cassette holder, followed by the Whatman paper, the gel, the membrane (the labelled side facing the gel), again Whatman paper and 2 or 3 sponges. If two gels are used, one sponge instead of 2 or 3 sponges are put in place after the Whatman paper, followed by Whatman paper, the second gel, the second membrane (the labelled side facing the gel), Whatman paper and 2 or 3 sponges. There should be no bubbles in the transfer stack.

The stack is placed in the electrophoresis chamber and the running buffer is replaced with the transfer buffer. The transferring step lasts for 1 h at 30 V for one gel and 1 h at 60 V for two gels at 4 °C. When the transfer is finished the weight markers on the membrane are labelled with a pen. Then the membrane is first rinsed in tap water for 5 min, shaking and then in blocking buffer (Table III) for 1 h, shaking. The membrane is then incubated with an appropriate diluted primary antibody in blocking buffer overnight on a rotor at 4°C.

The next day the membrane is washed three times with TBST, shaking for 5 min each. Then the membrane is incubated with HRP-conjugated secondary antibody (1:10000) in blocking buffer for one hour at room temperature. Next the membrane is again washed three times with TBST, shaking for 5 min each.

For the detection of horseradish peroxidase, chemiluminescent substrate is used. We used three different substrates:

- ECL: the substrate working solution is prepared by mixing Substrate A and Substrate B at a ratio of 1:1
- ECL Plus: the substrate working solution is prepared by mixing Substrate A and Substrate B at a ratio of 40:1
- Luminata: ready to use.

The membrane is incubate with 2 ml with one of these substrates at RT. The incubation time depends on the substrate used. The ECL is the weakest and Luminata is the strongest substrate. The membrane is removed from the working solution and placed in a film cassette with the protein side facing up. The cassette is closed and transported to the darkroom. In the darkroom all of the lights are turned off except the red light, which is appropriate for exposure. The film is placed on top of the membrane. The exposure time depends on intensity of the signal and needs to be adjusted to achieve optimal results. The film is developed by X-Omat 2000 processor. After the film is developed the membrane is washed in TBST, shaking for 1 min. It is then incubated with stripping buffer at 50 °C for 30 min, shaking. Afterwards it is washed in TBST and the next primary antibody can be applied.

3.2.4 Subcellular fractionation

Cells are grown in flasks in their corresponding culture media. 30 million cells are required.

Cells are removed from flasks using Trypsin EDTA as explained in the cell passaging section (3.2.1.1 above). Resuspension cells are transferred to a falcon tube and centrifuged at 1400 rpm for 5 min at room temperature. The supernatant is carefully removed with a vacuum pump without touching the cell pellet. Cells are resuspended in 1 ml of fresh culture media. A Neubauer chamber is used for cell counting. A coverslip is placed in the middle of the chamber and 10 µl of diluted cells (1:1000) are added. The chamber is placed under the microscope with a 10x objective. The chamber contains four corner squares and cells are counted in each of them. For each corner cells that are overlapping the top and left lines are included in counting and cells that are overlapping the bottom and right lines are not included. Cell counting is crucial if we have more samples that we want to compare in following experiments, like western blotting, because it enables that the same amount of cells is taken from each sample.

Cells per millilitre are calculated from following equation:

$$\text{Cells/ml} = \text{average count per square} \times \text{dilution factor} \times 10^4$$

An equal amount of cells are transferred from falcon tubes to Eppendorf tubes and centrifuged at 1400 rpm for 5 min at room temperature. The supernatant is removed with a

vacuum pump and the cell pellet is washed (the pellet is centrifuged at 1400 rpm for 5 min) with 1 ml of PBS, containing 0.4% BSA. The supernatant is removed with a vacuum pump and 200 μ l of complete cytosolic extraction buffer (CCEB, Table IV) with digitonin (0.625 mg/ml) is added to the cell pellet. The pellet is resuspended and lysed on ice for 10 till 20 min. Every 3 to 4 min cells are mixed with a pipette to improve the effectiveness of the lysing.

Meanwhile 5 μ l of cells and 5 μ l Trypan blue are mixed in a new Eppendorf tube. The mixture is added to a cytoslide and covered with a coverslip. The cytoslide is observed under microscope to evaluate the percentage of permeabilized cells. The permeabilized cells are stained blue, because of the Trypan blue and the CEB lyse buffer. This process is repeated until more than 80% of cells are permeabilized.

Lysed cells are centrifuged at 700 g for 10 min at 4 °C. The pellet consists of nuclei and is discarded. The supernatant is transferred to a new Eppendorf tube and centrifuged at 7000 g for 30 min at 4 °C. The pellet after centrifugation consists of mitochondria. The pellet is washed twice with 500 μ l of cold PBS. Then it is lysed with 100 μ l of CCEB containing 1% SDS by boiling for 5 min at 95 °C. The samples are again centrifuged at 14000 rpm for 3 min at 4 °C. The supernatant contains mitochondria, the pellet is discarded. 19.5 μ l of the sample can be used immediately for western blotting or it can be stored at -20 °C.

The supernatant from the second centrifugation is ultracentrifuged at 21000 g for 1 h at 4 °C. The pellet consists of lysosomes and peroxisomes. Then 50 μ l of CCEB containing 1% SDS is added to the pellet and lysed by boiling for 5 min at 95 °C. After the samples have cooled, 19.5 μ l of sample can be used immediately for western blotting or stored at -20 °C. The supernatant from 21000 g centrifugation consists of cytosol. 9.5 μ l can be used immediately for western blotting or the samples are stored at -20 °C.

3.2.5 Immunofluorescence staining

Adherent cells are grown in a 24-well plate on coverslips in culture media at 37 °C and 5% CO₂. After they reached 80% confluence the media is removed with a vacuum, the coverslips are washed with 300 μ l PBS, and the cells are fixed with 4% paraformaldehyde (PFA) for 10 min. Afterwards the coverslips are again washed twice with PBS. To achieve membrane permeabilization, cells are treated with 0.05% saponin for 5 min. After washing

the coverslips again with PBS, they are taken from the 24-well plate to a ceramic plate and incubated with acetone at -20°C for 10 min.

Before transporting the coverslips back to the 24-well plate, fresh PBS is added to the wells. The cells are washed twice with PBS. The coverslips are transferred into a humidified chamber and 80 µl of blocking solution (Table III) per coverslip is applied. These are then incubated for one hour at room temperature.

When blocking is complete, the coverslips are left in the humidified chamber and the blocking solution is removed carefully by pipetting. The primary antibodies diluted in blocking solution are applied and incubated at 4 °C overnight.

The next day the coverslips are transferred to the 24-well plate and washed three times with PBS for 5 min. They are then transferred back into the humidified chamber and the secondary antibodies diluted in 3.5% BSA are applied. The secondary antibody is chosen dependent on the donor species of primary antibody and the desired fluorochrome. These are incubated for one hour at room temperature. Afterwards they are again washed three times with PBS in the 24-well plate, with 5 min for each wash. 4 µl of mounting media is put on each coverslip and the coverslips are inverted onto cytoslides. When the mounting media is dried, the coverslips are sealed with nail polish and stored protected from light at -4 °C until microscopy.

In cases where Mitotracker is used it is applied before fixing the cells with PFA. The Mitotracker is diluted in culture media (1:1000) and added to cells and incubated for 20 min at 37 °C. Afterwards cells are washed with PBS and are fixed with 4% PFA for 10 min at 37 °C. The coverslips are then prepared for the immunofluorescence staining procedure as described above.

Suspension cells are transferred into falcon tubes and counted as described above. For staining, 200000 cells are needed. The correct volume of cells is taken and transferred to a 15 ml falcon tube. Cells are centrifuged at 1400 rpm for 5 min at room temperature. Supernatant is removed with a vacuum pump and cells are resuspended with 100 µl of culture media. To attach the cells to a cytoslide, 100 µl of cells are well mixed and cytospun at 200 rpm for 2 min. For cytospinning a metal container, cytoslide, Whatman paper, and a cell container are used. Afterwards cells are fixed with 4% PAF for 10 min. Then slides are put in a glass staining chamber and washed with PBS. The

immunofluorescence staining procedure is the same as for adherent cells. The difference is that the suspension cells are on cytoslides and the adherent cells are on coverslips.

3.2.6 Immunohistochemistry staining

A tissue microarray slide is put in a glass staining chamber and heated in the oven at 52 °C overnight. The next day the slide is deparaffinised with Neo-clear solution. Neo-clear is not water soluble, therefore the dewaxed samples are rehydrated in a series of decreasing concentrations of alcohol; twice with 100% ethanol, once with 90%, 80%, 60%, and 40% ethanol, for 3 min each time. The slide is then washed twice with distilled water and immersed in PBS, for 3 min each time.

The slide is then transferred into a plastic chamber which contained DAKO target retrieval solution (diluted at a ratio of 1:10 in water). The solution increases staining intensity with primary antibodies. The chamber is put in a microwave and heated for 3 min, which is followed by 20 min of cooling. This procedure is repeated twice.

The slide is then transferred back into the glass staining chamber and twice immersed in distilled water and PBS, for 3 min each time. The slide is then moved to the humidified chamber. DAKO dual endogenous enzyme block is used as a blocking solution. Before use, the solution is equilibrated to room temperature. After 5 min of blocking the primary antibody is applied. Mouse anti-ATG12 antibody is diluted at a ratio of 1:100 in DAKO antibody diluent. The slide is incubated in the humidified chamber with the first antibody overnight at 4 °C.

The next day the slide is transferred back to the glass staining jar and immersed twice in PBS for 5 min. Then the slide is incubated with DAKO biotinylated secondary antibody for 15 min at room temperature. Afterwards the slide is again immersed twice in PBS for 5 min. To label secondary biotinylated antibody the slide is incubated with DAKO streptavidin alkaline phosphatase for 15 min at room temperature. Then the slide is again immersed twice in PBS for 5 min. Meanwhile the substrate working solution (Table III) is prepared. The working solution forms a permanent red reaction product at the site of the target antigen. The slide is incubated with 100 µl of the working solution. This is then observed under a light microscope for the appearance of red dots, which represented the investigated ATG12 protein. These appeared after 15 min. Then the slide is immersed

twice in PBS for 3 min. The tissue is counterstained with hematoxylin for 1 min and then washed with tap water. The slide is dried and cleaned. One drop of the aqueous mounting agent Aquatex is added on the slide and covered with a coverslip. The slide is stored at room temperature until microscopy.

3.2.7 Quantification of the results from co-localization analysis

Images taken with the confocal microscope are analysed with Imaris 7.5.0. software. It measures the correlation of intensity distribution between two channels. To evaluate the co-localization of two variables, Pearson's correlation coefficient (R) is used. R measures the linear correlation between two variables and its values vary between -1 and 1. 1 means a perfect positive correlation between the two values and -1 means a perfect negative correlation between the two values. Values that are close to 1 or -1 indicate a possible correlation between the two variables. A result of 0 means there is no linear relationship between the two variables.

3.2.8 Statistical analysis

Analysis of all data are performed by the GraphPad Prism 5 software. All data is presented as means \pm SDs. Results are analysed using unpaired Student's t-test. Values of $p < 0.05$ are considered as statistically significant.

4 RESULTS

4.1 Mitochondrial localization of ATG12

Interesting findings regarding ATG12 have recently been discovered by host research group. The localization of ATG12 on mitochondria was determined with an immunofluorescence staining procedure by co-staining ATG12 with Mitotracker (specific marker for mitochondria) or anti-mitochondria (MTC) antibody. Co-localization was confirmed with high values of Pearson's correlation coefficient. The ATG12 staining pattern was very specific and not typical for any other ATG proteins. Interestingly, the Pearson's correlation coefficient was very low after co-staining with anti-ATG5 and anti-ATG12 antibodies. Subcellular fractionation was then performed to separate the mitochondrial fraction from the cytosolic fraction. After immunoblotting with anti-ATG12 antibody, ATG12 was detected only in the mitochondrial fraction, as a conjugate with ATG5. This supported the results of immunofluorescence staining, that is, the localization of ATG12 on mitochondria (49).

Our first goal was to confirm mitochondrial localization of ATG12 in liver cancer HepG2, T lymphoblastoid CEM cells and breast cancer MDA-MA-231 cells.

First we performed immunofluorescence staining with all three cell lines and a confocal laser scanning microscope was used to study the stained cells. To measure the level of co-localization between two proteins, the amount of co-localized puncta has to be quantified. As a statistic to represent the level of co-localization we used Pearson's correlation coefficient (R). The R value was calculated with computer software. It represents the co-localized signal from overlapping signals from different fluorescence channels. Results were presented as the mean of R values obtained from analysed images, with standard deviation and 95% confidence interval.

To confirm the localization of ATG12 on mitochondria, we co-stained ATG12 and mitochondria in HepG2 and MDA-MA-231 cell lines. For mitochondria staining, a specific mitochondria marker Mitotracker was used. ATG12 was detected with anti-ATG12 antibody. High values of Pearson's correlation coefficient in both cell lines indicated a possible co-localization of ATG12 and mitochondria: $R_{\text{HepG2}}=0.651\pm 0.043$, $R_{\text{MDA-MA-231}}=0.735\pm 0.059$ (Figure 4).

In addition co-localization of ATG12 and mitochondria was investigated using anti-SSBP1 antibody, which is another mitochondria marker. SSBP1 (single-stranded DNA binding protein 1) is a specific mitochondrial protein and is involved in mitochondrial biogenesis and associates with mitochondrial DNA (50). The high values of Parsons's correlation coefficient in HepG2 and CEM cells ($R_{\text{HepG2}}=0.643\pm 0.071$, $R_{\text{CEM}}=0.601\pm 0.029$) confirmed our assumption of ATG12 localization on mitochondria (Figure 5).

To eliminate the possibility of ATG12 being a part of the lysosome or ER, we co-stained ATG12 with LAMP1 and ERAP1. LAMP1 (Lysosomal-associated membrane protein 1) is located on the lysosome and ERAP1 (Endoplasmic reticulum aminopeptidase 1) associates with ER. As expected the values of Pearson's correlation coefficient were very low ($R_{\text{LAMP1}}=0.060\pm 0.060$, $R_{\text{ERAP1}}=0.090\pm 0.065$), confirming our expectation that it is unlikely that ATG12 is located on the lysosome or on ER (Figure 6).

In addition we also co-stained ATG12 and LC3 to investigate whether ATG12 co-localizes with LC3 on the autophagosomal membrane. The results showed low correlation ($R_{\text{LC3}}=0.118\pm 0.085$) between ATG12 and LC3 puncta, indicating that a small amount of ATG12 is located on the autophagosomal membrane (Figure 6).

We compared Parsons's correlation coefficient between ATG12 and Mitotracker with ATG12 and LAMP1, ERAP1 and LC3. The difference was significant ($p<0.001$) in all three cases, confirming our hypothesis that ATG12 is located on mitochondria (Figure 7).

To further confirm localization of ATG12 on mitochondria and to study the effect of autophagy on cellular ATG12 expression we performed subcellular fractionation and immunoblotting. First, cells were exposed to four different conditions; they were either untreated or treated with starvation media (EBSS media), Chloroquine (CQ) or a combination of CQ in starvation media. Untreated cells were left in culture media (DMEM media) and were used as control. Autophagy was induced by treating cells with starvation media (EBSS media). By using CQ, fusion of autophagosome with lysosome was prevented (29). With subcellular fractionation mitochondrial fraction was separated from the cytosolic fraction. Successful fractionation was confirmed with immunoblotting using organelle specific antibodies. For mitochondria anti-MTC02 (anti-mitochondria) antibody was used, it was detected only in the mitochondrial fraction, indicating a relative pure

fraction. GAPDH is a cytosolic protein and is used as a loading control to ensure the same amount of proteins in each sample (Figure 8).

ATG12 was detected only in the mitochondrial fraction at a molecular weight around 55 kDa, as an ATG12-ATG5 conjugate. ATG5 was detected in the cytosolic fraction and not in the mitochondrial fraction, indicating that the anti-ATG5 antibody we used, detects only the ATG12-ATG5 conjugate that is located in the cytosol. Interestingly the strongest ATG12 band was detected in the control cells and the weakest under starvation conditions. The ATG12 band with CQ treatment is slightly stronger than the band with CQ in starvation media treatment (Figure 8).

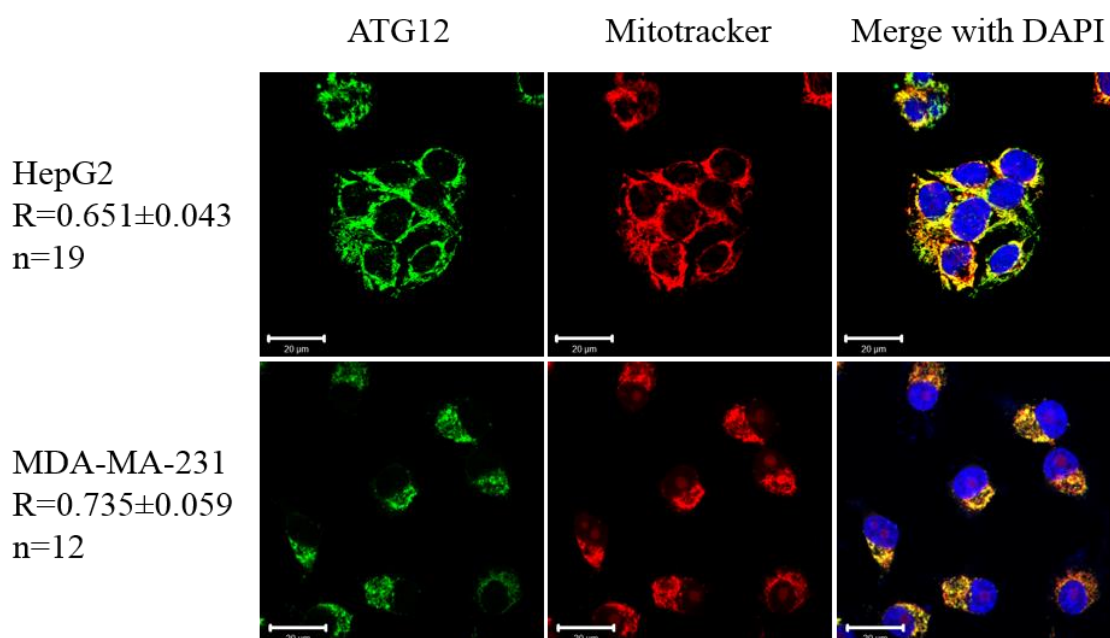


Figure 4: ATG12 was co-localized with Mitotracker in HepG2 and MDA-MA-231 cells. Liver cancer HepG2 and breast cancer MDA-MA-231 cells were seeded on coverslips and incubated at 37°C in DMEM media in a 24-well plate. After they reached 80% confluence they were stained with Mitotracker (1:1000) and incubated at 37°C for 15 min. They were fixed with 4% PFA for 10 min at 37°C. Process was continued with the immunofluorescence staining protocol and cells were stained with mouse anti-ATG12 (1:50) antibody. Stained cells were observed under LSM confocal microscope. Pictures were analysed with Imaris software which calculated the value of Pearson's correlation coefficient. n represents the number of analysed pictures. Scale: 20um

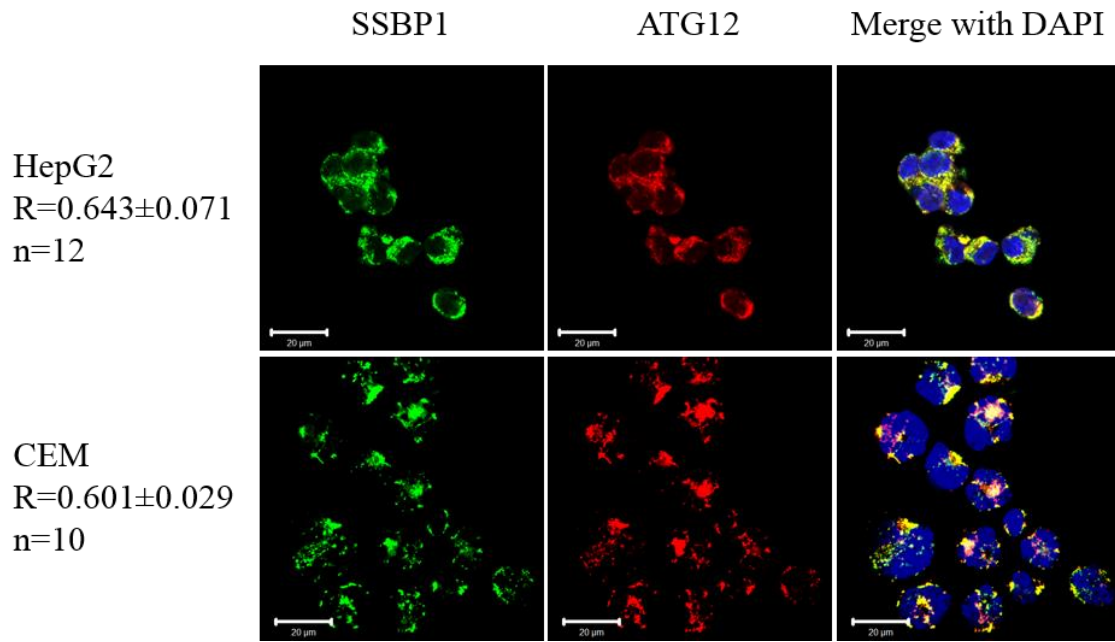


Figure 5: ATG12 was co-localized with SSBP1 in HepG2 and CEM cells. HepG2 cells were seeded on coverslips and incubated at 37°C in DMEM media in a 24-well plate. After they reached 80% confluence they were fixed with 4% PFA for 15 min at room temperature. Process was continued with the immunofluorescence staining protocol and cells were stained with mouse anti-ATG12 (1:50) and rabbit anti-SSBP1 (1:100) antibodies. 200000 CEM cells were cytopspined and fixed with 4% PFA for 10 min. Process was continued with the immunofluorescence staining protocol and cells were stained with mouse anti-ATG12 (1:50) and rabbit anti-SSBP1 (1:100) antibodies. Stained cells were observed under LSM confocal microscope. Pictures were analysed with Imaris software which calculated the value of Pearson's correlation coefficient. n represents the number of analysed pictures. Scale: 20um

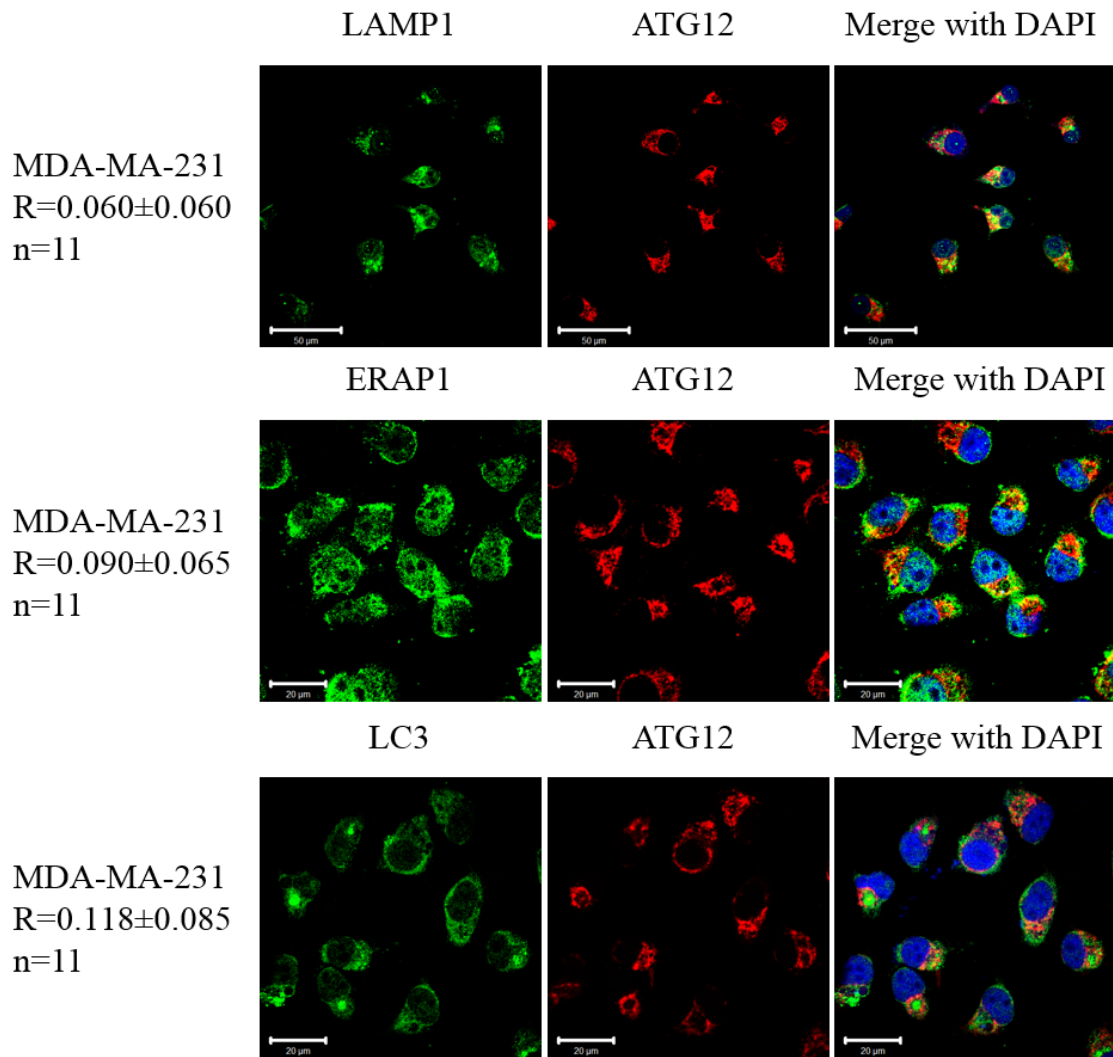


Figure 6: ATG12 was not co-localized with LAMP1, ERAP1 and LC3 in MDA-MA-231 cells. MDA-MA-231 cells were seeded on coverslips and incubated at 37°C in DMEM media in a 24-well plate. After they reached 80% confluence they were fixed with 4% PFA for 15 min at room temperature. Process was continued with the immunofluorescence staining protocol and cells were stained with mouse anti-ATG12 (1:50) and rabbit anti-SSBP1 (1:100), rabbit anti-ERAP1 (1:100) and rabbit anti-LC3 (1:100) antibodies. Stained cells were observed under LSM confocal microscope. Pictures were analysed with Imaris software which calculated the value of Pearson's correlation coefficient. n represents the number of analysed pictures. Scale: 20um

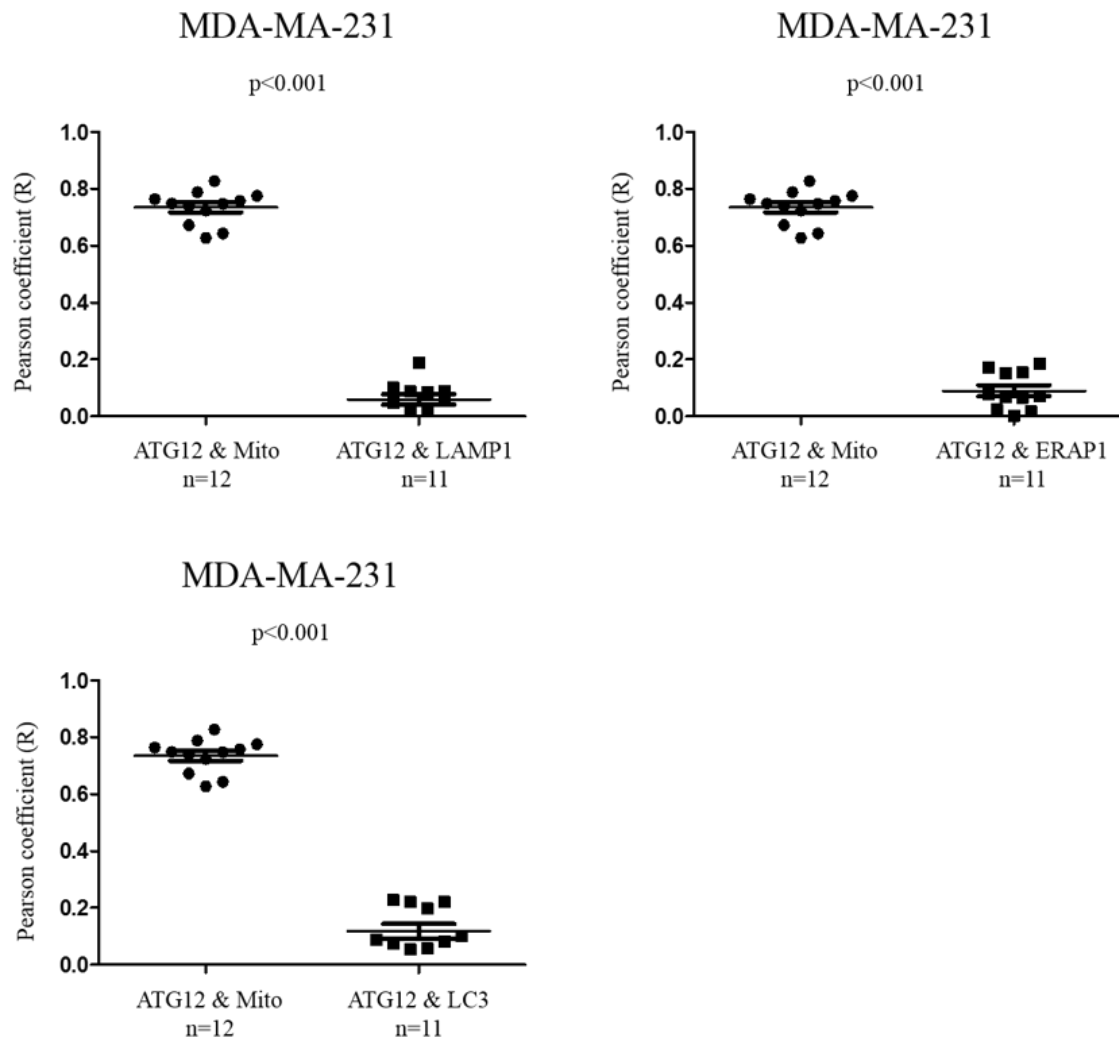


Figure 7: Significant difference in co-localization between ATG12 and Mitotracker with ATG12 and LAMP1, ERAP1 and LC3 in MDA-MA-231 cells. The Pearson's correlation coefficient (R) values of ATG12 staining with Mitotracker were compared to ATG12 staining with LAMP1, ERAP1 and LC3. Values of Pearson's correlation coefficient were analysed with GraphPad Prism 5 and presented as means \pm SDs. Unpaired Student's t test was used to gain the two-tailed p values. Values of $p < 0.05$ were considered statistically significant. n represents the number of analysed pictures.

HepG2

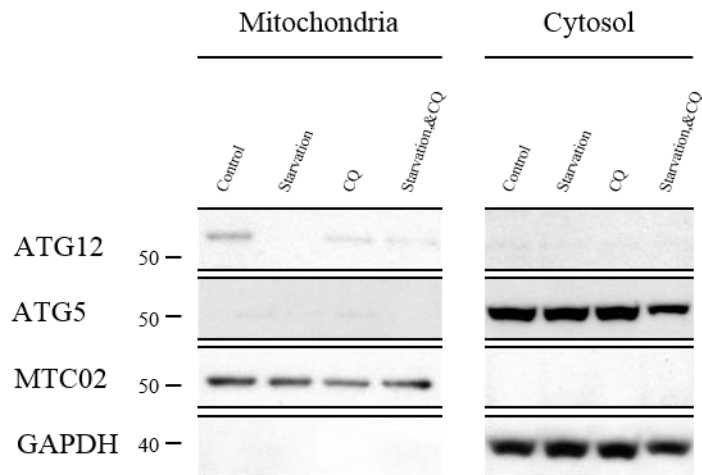


Figure 8: ATG12 is present in the mitochondrial fraction. For one hour liver cancer HepG2 cells were either untreated or treated with starvation media (EBSS), CQ and a combination of CQ in starvation media (1:10000 in EBSS media). Per condition 30 million HepG2 cells were used for subcellular fractionation. Protein samples were applied on 12% SDS-PAGE gel and transferred to a polyvinylidene difluoride (PVDF) membrane. The membrane was blotted with anti-ATG12 (1:1000), anti-ATG5 (1:1000), anti-MTC02 (1:1000), anti-GAPDH (1:10000) antibodies. HRP-conjugated secondary antibodies were added and proteins were detected based on the chemiluminescent method with the X-omat 2000 processor. Successful isolation of mitochondrial fraction was demonstrated by the presence of MTC02 in the mitochondrial fraction. GAPDH was used as loading control.

4.2 Mitochondrial localization of ATG12 is independent on Bcl-2

The main aim of my thesis was to define whether mitochondrial localization of ATG12 is dependent on Bcl-2. Bcl-2 is an anti-apoptotic protein and is mainly found on the membrane of ER and on the outer mitochondrial membrane (51). For this experiment suspension T lymphoblastoid CEM cell line was used. To study the dependency on Bcl-2 we used wild type and Bcl-2 overexpressing CEM cells, which were kindly provided by Dr. S. Martin (52).

To investigate if mitochondrial localization of ATG12 was dependent on Bcl-2, we performed immunofluorescence staining and immunoblotting with CEM wild type (CEM_{WT}) and Bcl-2 overexpressing (CEM_{Bcl-2}) cells.

CEM wild type and Bcl-2 overexpressing cells were co-stained with anti-ATG12 and anti-SSBP1 antibodies. After observing cells under the confocal microscope, Pearson's correlation coefficients were calculated. In both cell types high values of Pearson's correlation coefficient were determined. Microscopic observation did not reveal any obvious difference in the staining pattern of mitochondria, ATG12 or in the morphology of cells and neither was there a difference in the fluorescence signal intensity between CEM_{WT} and CEM_{Bcl-2} cells. Our observations suggested an independent relationship between localization of ATG12 on mitochondria and Bcl-2 (Figure 9A).

Furthermore we compared Pearson's correlation coefficients of wild type and Bcl-2 overexpressing CEM cells. The p value (p=0.0549) was not as high as expected. However, because we did not see any difference in the staining pattern, cell morphology or signal intensity during the microscopic observation we can assume an independent relationship between mitochondrial localization of ATG12 and Bcl-2 (Figure 9B).

To confirm our assumption we performed subcellular fractionation and immunoblotting with wild type and Bcl-2 overexpressing CEM cells. Again we separated the mitochondrial fraction apart from cytosolic fraction. Lysosomal protein LAMP1 was detected with the anti-LAMP1 antibody, and its absence in the mitochondrial fraction implies a relative clear fraction. Effective separation was also confirmed with the detection of mitochondria specific MTC protein in the mitochondrial fraction. Unfortunately the MTC band in the mitochondrial fraction of CEM_{WT} cells was very weak. Since we did not see any difference

in mitochondrial expression between CEM_{WT} and CEM_{Bcl-2} cells when observing under microscope, we thought that a weak MTC band could be due to losing proteins because of the stripping buffer that was used several times to remove antibodies. Successful overexpression of Bcl-2 was shown with anti-Bcl-2 antibody. The Bcl-2 band in CEM_{Bcl-2} cells, was very strong, whereas the band in CEM_{WT} cells was barely visible. ATG12 was detected in mitochondrial fractions in both cell types and their bands were equally strong. The results indicate an independent relationship between ATG12 mitochondrial localization and the anti-apoptotic Bcl-2 protein. The data correspond to the results of immunofluorescence staining, confirming our hypothesis that mitochondrial localization of ATG12 is Bcl-2 independent (Figure 10).

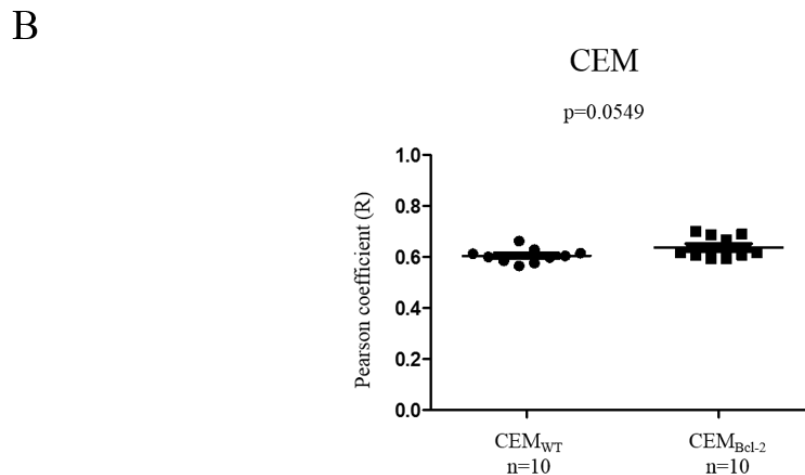
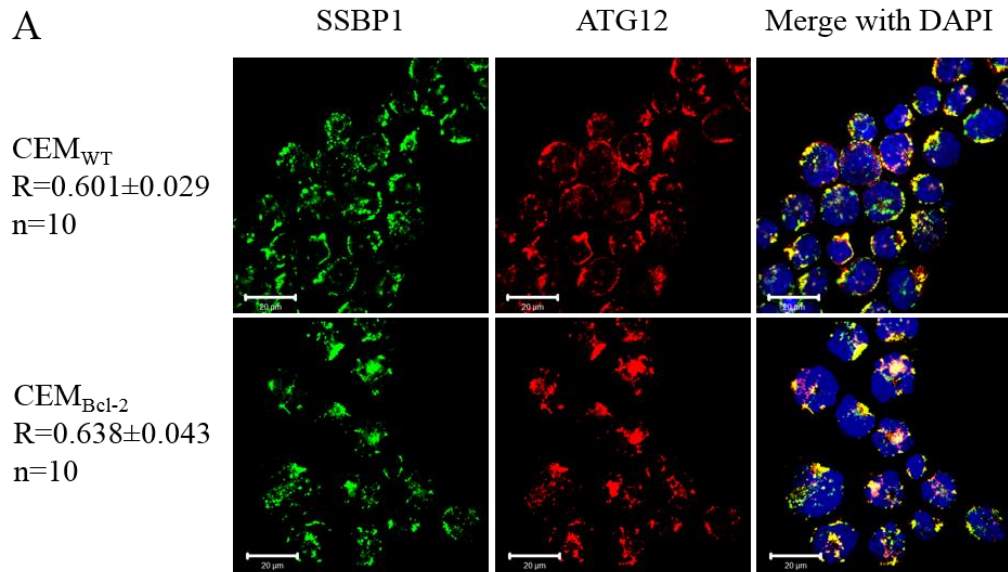


Figure 9: Mitochondrial localization of ATG12 is independent on Bcl-2 overexpression in CEM cells. (A) Immunofluorescence staining of ATG12 and mitochondria in wild type and Bcl-2 overexpressing CEM cells. 200000 CEM cells were cytopspined and fixed with 4% PFA for 10 min. Process was continued with the immunofluorescence staining protocol and cells were stained with mouse anti-ATG12 (1:50) and rabbit anti-SSBP1 (1:100) antibodies. Stained cells were observed under LSM confocal microscope. Pictures were analysed with Imaris software which calculated the value of Pearson's correlation coefficient. n represents the number of analysed pictures. Scale: 20um. **(B) Statistical evaluation of ATG12 mitochondrial localization in CEM_{WT} and CEM_{Bcl-2} cells.** The Pearson's correlation coefficient (R) values of ATG12 and mitochondria staining with mouse anti-ATG12 and rabbit anti-SSBP1 antibodies were compared between wild type and Bcl-2 overexpressing CEM cells. Values of Pearson's correlation coefficient were analysed with GraphPad Prism 5 and presented as means ± SDs. An unpaired Student's t test was used to gain the two-tailed p values. No significant difference in mitochondrial localization of ATG12 between wild type and Bcl-2 overexpressing CEM cells was determined. Values of $p < 0.05$ were considered statistically significant. n represents the number of analysed pictures.

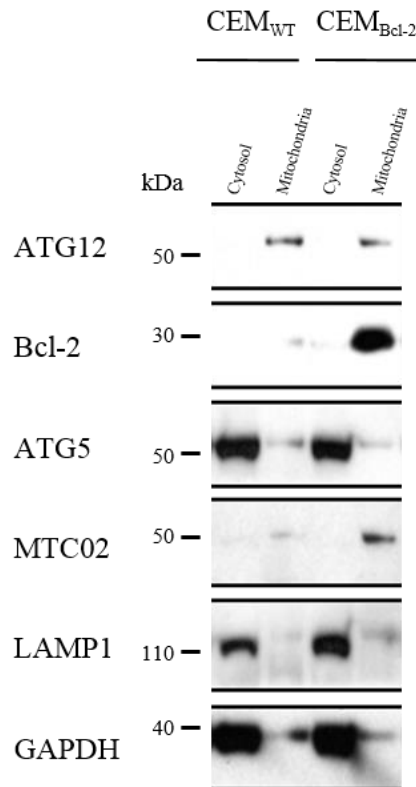


Figure 10: Independency of ATG12 mitochondrial localization on Bcl-2 overexpression in CEM cells is shown with immunoblotting. CEM cells were grown in culture media. Per type, 30 million CEM cells were used for subcellular fractionation. Protein samples were applied on 12% SDS-PAGE gel and transferred to a polyvinylidene difluoride (PVDF) membrane. The membrane was blotted with anti-ATG12 (1:1000), anti-Bcl-2 (1:1000), anti-ATG5 (1:1000), anti-MTC02 (1:1000), anti-LAMP1 (1:1000), anti-GAPDH (1:10000) antibodies. HRP-conjugated secondary antibodies were added and proteins were detected based on the chemiluminescent method with the X-omat 2000 processor. Effective overexpression of Bcl-2 is shown with a stronger band in CEM_{Bcl-2} cells than in CEM_{WT} cells. Successful isolation of mitochondrial fraction was demonstrated by the presence of MTC02 in the mitochondrial fraction and the absence of LAMP1 in the mitochondrial fraction. GAPDH was used as loading control.

4.3 Cellular expression of ATG12 in tumor and normal tissues

A decreased expression of ATG5 in melanoma cells in comparison with benign nevi and normal skin cells was recently determined in host research group (46). Therefore we decided to investigate whether there is also a difference in the expression of ATG12 between tumor and normal tissues.

First we performed immunofluorescence staining of normal fibroblasts. We used anti-ATG12 antibody to detect our protein and anti-SSBP1 antibody to detect mitochondria. As we can see on Figure 11, the expression of ATG12 in fibroblasts was much lower than in liver cancer HepG2 cells. Also, expression of mitochondria was stronger than the ATG12 expression in fibroblasts. Interestingly the value of Pearson's correlation coefficients ($R_{\text{fibroblasts}}=0.309\pm 0.081$) in normal fibroblasts was lower than in liver cancer HepG2, T lymphoblastoid CEM, and breast cancer MDA-MA-231 cells. Which could mean a difference in ATG12 co-localization with mitochondria between cancer HepG2, MDA-MA-231 and CEM cells and normal fibroblasts. As a result of the weak ATG12 signal, it was difficult to analyse the pictures with the computer software and this could also be one of the reasons for the low R value (Figure 11).

To further investigate the expression of ATG12 in tumors, we used tissue microarray (TMA) technology. It enables analysis of up to 600 tissue samples on one slide and in a relatively short time (53). Our TMA contained 564 tissue samples of 21 different organs. Samples were taken from different patients. From each patient two samples from tumor tissue and two from its corresponding normal tissue were taken. Immunohistochemistry staining was performed with anti-ATG12 antibody. Pictures were taken with a light microscope. ATG12 positive (stained in red as punctations) and negative cells were manually counted and the percentage of ATG12 positive cells was calculated. The mean percentage of ATG12 positive cells were calculated for normal and tumor tissues taken from the same organ. Results are presented as mean percentage of ATG12 positive cells in tumor and normal tissues (Table V). The p values were obtained to evaluate the difference of ATG12 expression in tumor and normal tissues. Values of $p < 0.05$ were considered statistically significant.

In colon, mammary gland, prostate, lung, skeletal muscle, esophagus, testicle and stomach we could see a significant difference in ATG12 expression between their cancer and

normal tissues (Figures 12B and 13B). As we can see in Figures 12A and 13A there is an increased expression of ATG12 in tumor tissues in comparison to their paired normal tissues. Controversially, in some liver and kidney samples we could see highly expressed ATG12 in normal tissues and very low expression of ATG12 in tumor tissues. However the above stated tissues with statistically significant difference in ATG12 expression correlated with results from immunofluorescence staining of normal fibroblasts.

Table V: Mean percentages of ATG12 positive cells

Tissue type	% of ATG12 positive cells Number of samples (n)				p values
	Normal tissue	n	Cancer tissue	n	
Colon	12.59	10	81.50	10	<0.0001
Lung	10.13	10	54.75	10	0.004
Mammary gland	1.04	7	69.03	10	<0.0001
Prostate	14.16	3	73.92	9	0.0115
Esophagus	17.09	6	66.29	6	0.0141
Stomach	33.35	6	75.01	6	0.0175
Testicle	18.18	4	58.06	6	0.0179
Skeletal muscle	6.55	6	56.27	6	0.0126
Skin	4.50	2	46.55	5	0.191
Thyroid	38.09	6	46.84	5	0.748
Spleen	1.29	4	3.50	7	0.522
Kidney	58.85	6	41.74	6	0.432
Ovaries	20.04	5	49.02	4	0.213
Uterus	2.03	6	24.58	5	0.080
Liver	65.53	6	65.74	6	0.993
Brain	23.87	2	45.30	8	0.515
Appendix	9.33	10			
Lymph node	18.50	6			
Tonsil	14.46	10			
Placenta	50.10	6			
Salivary gland	22.55	6			
Mamma DISC	18.34	6			

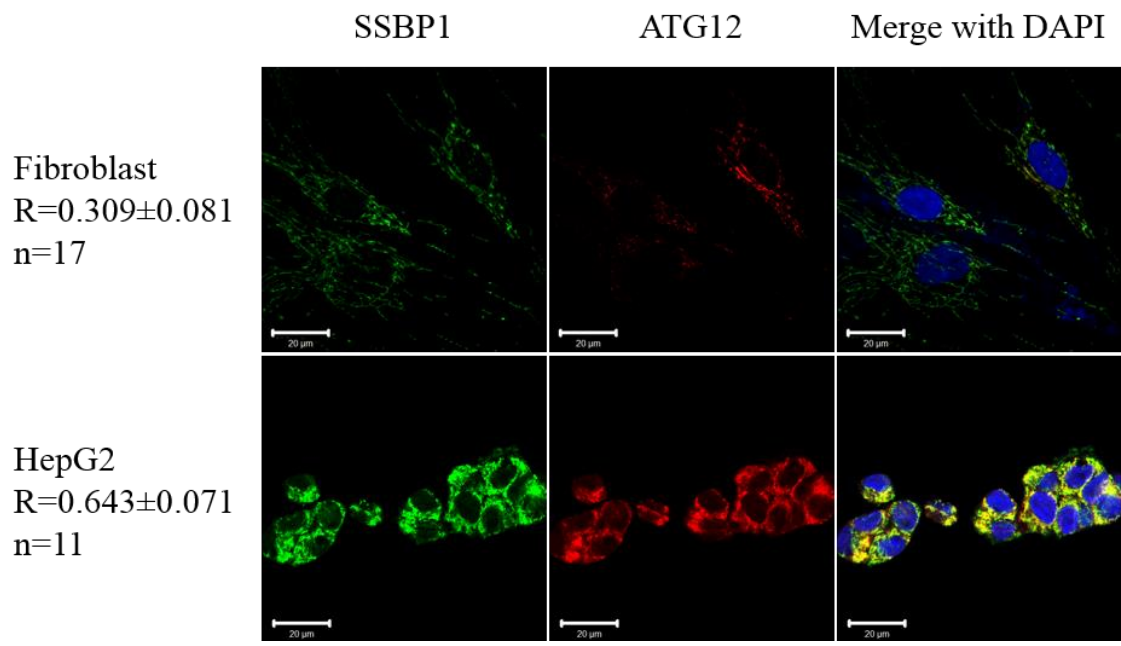


Figure 11: Lower ATG12 expression in normal fibroblasts in comparison to liver cancer HepG2 cells. Liver cancer HepG2 cells and fibroblast cells were seeded on coverslips and incubated at 37°C in DMEM media in a 24-well plate. After they reached 80% confluence they were fixed with 4% PFA for 15 min at room temperature. Process was continued with the immunofluorescence staining protocol and cells were stained with mouse anti-ATG12 (1:50) and rabbit anti-SSBP1 (1:100) antibodies. Stained cells were observed under LSM confocal microscope. Pictures were analysed with Imaris software which calculated the value of Pearson's correlation coefficient. n represents the number of analysed pictures. Scale: 20um

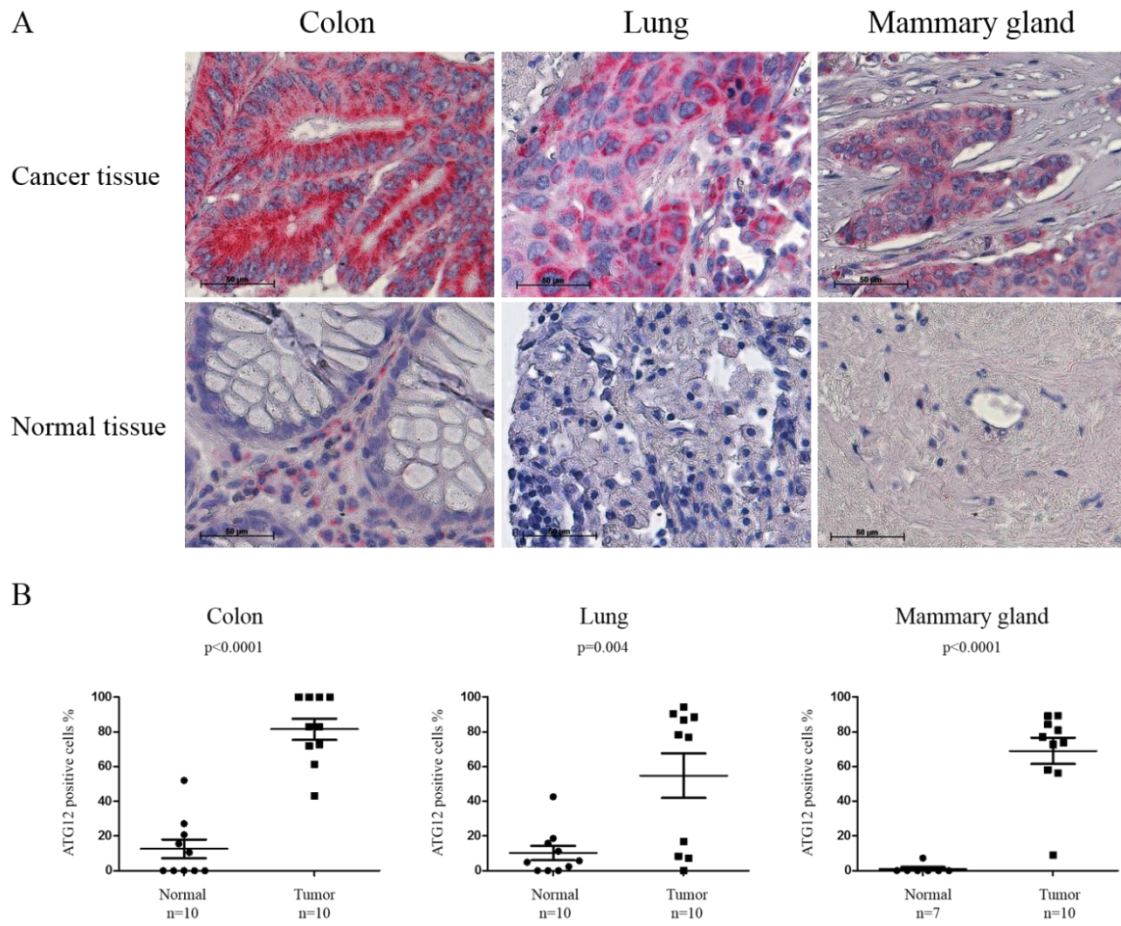


Figure 12: Significantly increased expression of ATG12 in colon, lung and mammary gland tumors tissues in comparison to their corresponding normal tissues. (A) Immunohistochemistry staining of ATG12 in colon, lung and mammary gland tumors tissues and their corresponding normal tissues. For comparison of ATG12 expression in tumor and normal tissues, tissue microarray (TMA) technology was used. TMA slide with different samples of normal and tumor tissues was stained with mouse anti-ATG12 (1:50) antibody following immunohistochemistry staining procedure. The pictures were taken with Zeiss Axiovert 35 light microscope. Scale: 50um. **(B) Statistical evaluation of ATG12 expression in normal and tumor tissues of colon, lung and mammary gland.** Mean percentage of ATG12 positive cells from normal and tumor tissues were compared. Mean percentage of ATG12 positive cells were analysed with GraphPad Prism 5 and presented as means \pm SDs. An unpaired Student's t test was used to gain the two-tailed p values. Significant difference in percentage of ATG12 positive cells was determined in colon, lung and mammary gland tumors tissues in comparison to their corresponding normal tissues. Values of $p < 0.05$ were considered statistically significant. n represents the number of analysed tissues.

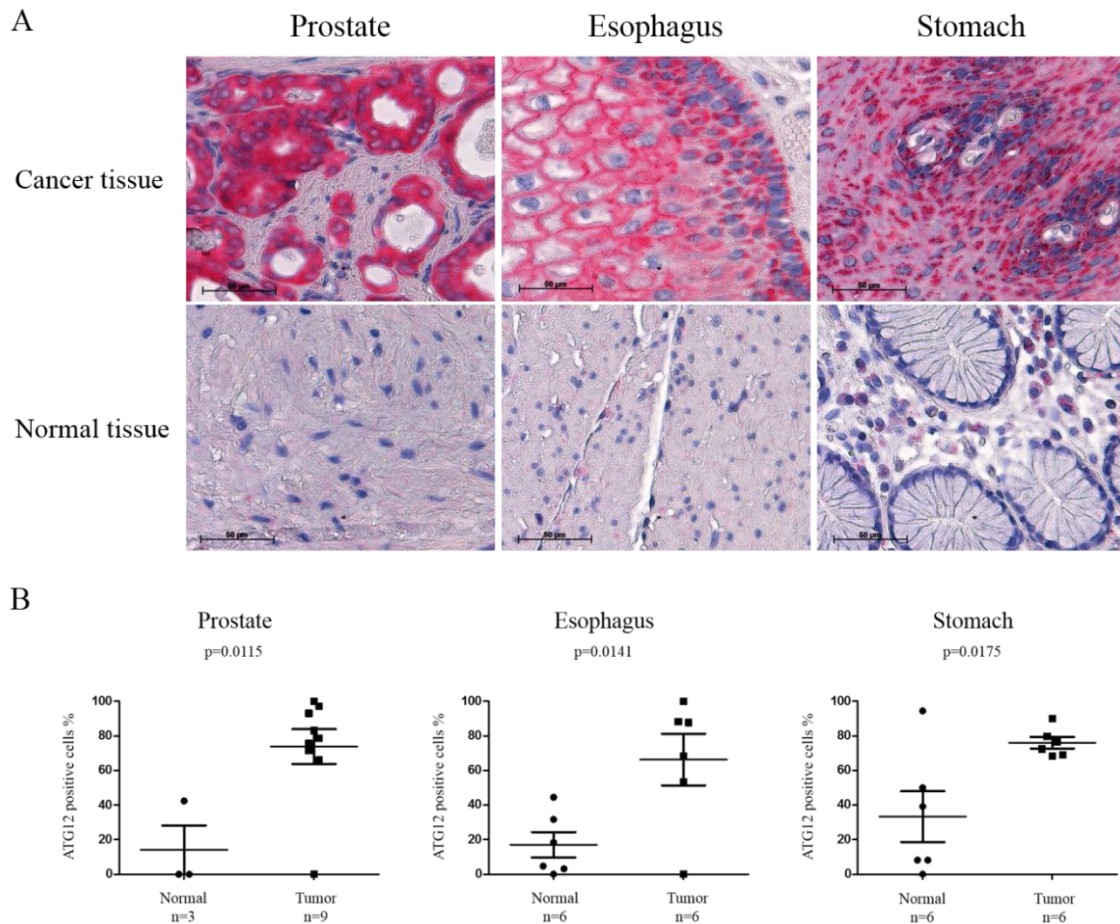


Figure 13: Significantly increased expression of ATG12 in prostate, esophagus and stomach tumors tissues in comparison to their corresponding normal tissues. (A) Immunohistochemistry staining of ATG12 in prostate, esophagus and stomach tumors tissues and their corresponding normal tissues. For comparison of ATG12 expression in tumor and normal tissues, tissue microarray (TMA) technology was used. TMA slide with different samples of normal and tumor tissues was stained with mouse anti-ATG12 (1:50) antibody following immunohistochemistry staining procedure. The pictures were taken with Zeiss Axiovert 35 light microscope. Scale: 50um. **(B) Statistical evaluation of ATG12 expression in normal and tumor tissues of prostate, esophagus and stomach.** Mean percentage of ATG12 positive cells from normal and tumor tissues were compared. Mean percentage of ATG12 positive cells were analysed with GraphPad Prism 5 and presented as means \pm SDs. An unpaired Student's t test was used to gain the two-tailed p values. Significant difference in percentage of ATG12 positive cells was determined in prostate, esophagus and stomach tumors tissues in comparison to their corresponding normal tissues. Values of $p < 0.05$ were considered statistically significant. n represents the number of analysed tissues.

4.4 Cytosolic and mitochondrial ATG12-ATG5 conjugate

We performed subcellular fractionation with lung cancer H1299 cells, breast cancer MDA-MA-231 cells and liver cancer HepG2 cells. Cells were grown in their corresponding culture media. Again we separated mitochondrial fraction from the cytosolic fraction. Successful separation was confirmed with the absence of LAMP1 in mitochondrial fraction. Also, anti-MTC02 antibody was detected only in the mitochondrial fraction. Unfortunately we were not able to detect MTC02 in breast cancer MDA-MA-231 cells. Protein samples of breast cancer MDA-MA-231 cells that we used for this experiment were previously used in a western blot. There a MTC02 band was seen and detected only in the mitochondrial fraction, indicating a clear mitochondrial fraction. Loss of MTC02 signal could be due to losing proteins, because of the stripping buffer that was used several times to remove antibodies from the membrane, before applying anti-MTC02 antibody (Figure 14).

We detected ATG12 with mouse and rabbit anti-ATG12 antibody. As before, with mouse anti-ATG12 antibody we detected ATG12 only in the mitochondrial fraction. The rabbit anti-ATG12 antibody detects the same ATG12-ATG5 conjugate as mouse anti-ATG5 antibody. As we can see on the film the mitochondrial ATG12 band is slightly higher than the cytosolic band detected with rabbit anti-ATG12, indicating a difference in molecular weight between the ATG12-ATG5 conjugate detected with mouse anti-ATG12 antibody and the one which was detected with rabbit anti-ATG12 antibody (Figure 14).

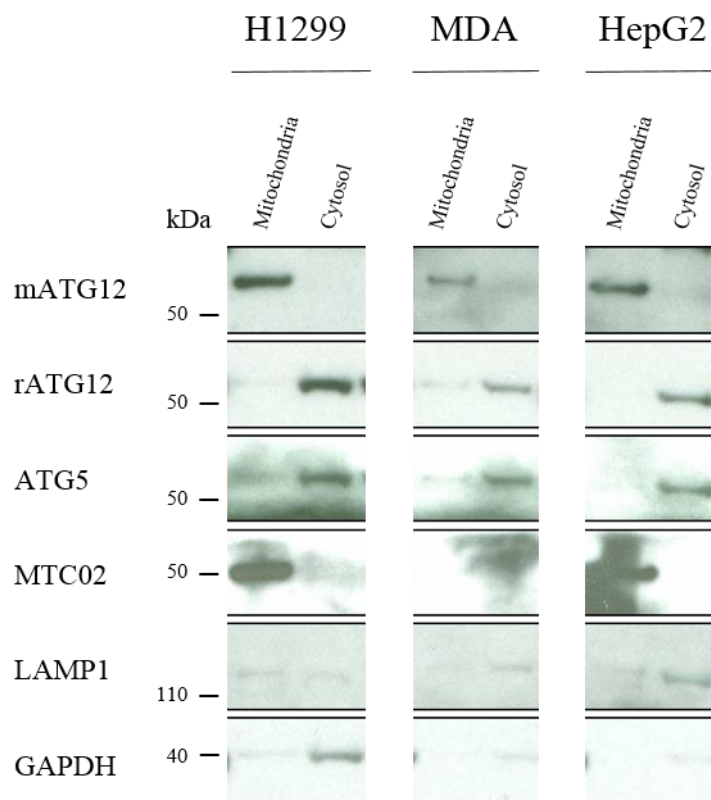


Figure 14: Different molecular weights of ATG12-ATG5 conjugates detected with mATG12 and rATG12 antibodies. 30 million lung cancer H1299, breast cancer MDA-MA-231 and liver cancer HepG2 cells were used for subcellular fractionation. Protein samples were applied on 12% SDS-PAGE gel and transferred to a polyvinylidene difluoride (PVDF) membrane. The membrane was blotted with mouse anti-ATG12 (1:1000), rabbit anti-ATG12 (1:1000), mouse anti-ATG5 (1:1000), mouse anti-MTC02 (1:1000), rabbit anti-LAMP1 (1:1000), and mouse anti-GAPDH (1:10000) antibodies. HRP-conjugated secondary antibodies were added and proteins were detected based on the chemiluminescent method with the X-omat 2000 processor. Successful isolation of mitochondria fraction was demonstrated by the presence of MTC02 in the mitochondrial fraction and the absence of LAMP1 in the mitochondrial fraction. GAPDH was used as loading control.

5 DISCUSSION

The aim of my thesis was to further characterize autophagy-related protein 12. I confirmed the mitochondrial localization of ATG12. Furthermore I determined that the mitochondrial localization of ATG12 is Bcl-2 independent.

We confirmed the hypothesis of ATG12 localization on the mitochondria using immunofluorescence staining and immunoblotting techniques. Co-localization of ATG12 with Mitotracker and SSBP1 was proven with high Pearson's correlation coefficient values in liver cancer HepG2, breast cancer MDA-MA-231 and T lymphoblastoid CEM cells. The R values varied between the cell lines. The highest R value was in MDA-MA-231 cells (R=0.735).

We excluded the possibility of ATG12 being part of the lysosome and ER based on the very low Pearson's correlation coefficients ($R_{LAMP1}=0.060$, $R_{ERAP1}=0.090$). These values were calculated from ATG12 co-stained with LAMP1 and ERAP1 in breast cancer MDA-MA-231 cells.

Based on these results we confirmed the hypothesis of mitochondrial localization of ATG12. The R value between ATG12 and LC3 ($R_{LC3}=0.118$) indicates that a small amount of ATG12 is located on the autophagosomal membrane; however, the results show that the majority of ATG12 is located on the mitochondria.

Mitochondrial localization of ATG12 was also confirmed with subcellular fractionation and immunoblotting, in liver cancer HepG2 cells. ATG12 was detected only in the mitochondrial fraction as an ATG12-ATG5 conjugate. The strongest ATG12 band was seen in the control cells and the weakest under starvation conditions. The ATG12 band for cells treated with CQ was slightly stronger than the band with CQ in starvation media treated cells. Interestingly, different conditions did not affect levels of detected ATG5, except in cells treated with CQ in starvation media, there a weaker ATG5 band was detected. It is difficult to make any conclusions whether this condition actually affects ATG5. Since we can see a weaker GAPDH band under the same condition, the reason could probably be that there a lower concentration of proteins was loaded. Also ATG5 was not detected in the same fraction as ATG12 using mouse anti-ATG12 antibody, which indicates that the antibody for detecting ATG12 is specific for the ATG12-ATG5

conjugate located on the mitochondria and the anti-ATG5 antibody used to detect ATG5 is specific for the conjugate located on the cytosol. Decreased levels of ATG12 and moderate changes of ATG5 after starvation-induced autophagy were also observed in a previous study that performed immunoblotting in colon cancer HCT116, lung cancer H1299 and breast cancer MDA-MA-231 cells (38).

To test whether we successfully induced autophagy and blocked the degradation process using CQ, we could have used LC3 immunoblotting. The amount of LC3 correlates well with the number of autophagosomes, thus it is widely used for monitoring autophagy. Following SDS-PAGE and immunoblotting, LC3 is detected as two bands. One represents cytosolic LC3-I and the other represents the lipidated LC3-II, which is located on the inner and outer autophagosomal membrane. Inducing autophagy with starvation media would show a stronger LC3-II band and a weaker LC3-I band. Treating cells with CQ in culture media would show an even stronger LC3-II band than for cells treated only with starvation media. The strongest LC3-II band would be detected in the cells treated with CQ in starvation media treated cells (54).

We used wild type and Bcl-2 overexpressing CEM cells to investigate the relationship between mitochondrial localization of ATG12 and Bcl-2. After immunofluorescence staining high values of Pearson's correlation coefficient were determined in CEM_{WT} and CEM_{Bcl-2} cells. Under the confocal microscope we could not see any difference in the staining pattern, cell morphology or signal intensity between CEM_{WT} and CEM_{Bcl-2} cells. The calculated p value was lower than expected; therefore, we performed subcellular fractionation and immunoblotting. ATG12 was equally strong detected in both cell types. Based on microscopical observations and immunoblotting results, we concluded that mitochondrial localization of ATG12 is Bcl-2 independent.

A recently published study showed the reduction of ATG5 expression in primary melanomas in comparison to benign nevi. Reduction of autophagy as a result of downregulation of ATG5 expression was also shown (46). We decided to investigate whether a difference in ATG12 expression could also be found. We saw a decreased expression of ATG12 in normal fibroblasts in comparison to liver cancer HepG2, T lymphoblastoid CEM and breast cancer MDA-MA-231 cells. These findings led us to further investigate ATG12 expression in tumors.

Our tissue microarray slide was stained with anti-ATG12 antibody following immunohistochemistry staining protocol. We could not quantify all of the TMA tissue samples. From certain organs we only had samples from normal tissues without their paired tumor tissues (Table V). Some of the tissue samples were damaged, therefore we could not consider them in the evaluation. Consequently, from certain organs we had relative low numbers of samples, thus it was not possible to make any statistical conclusions for these tissues. However, in 8 tissue types a statistically significant difference between ATG12 expression in tumor and normal tissues was observed. We could see a strong expression of ATG12 in tumor tissues, whereas in normal tissues ATG12 was very low expressed or even not detectable. On the contrary, in some liver and kidney tissues we observed a high level of ATG12 expression in normal tissues and a low expression in tumor tissues, suggesting that ATG12 expression is dependent on the tissue type.

We also need to consider that our TMA slide included tissue samples of different cancer subtypes taken from organs at different stages of the disease. The samples were categorized based on the organ they were taken from. But there were not enough samples to draw conclusions regarding ATG12 expression in the different stages of cancer or subtypes. However, in the colon, mammary gland, prostate, lung, skeletal muscle, esophagus, testicle and stomach tissues we could see a significant difference in ATG12 expression, between their cancer and normal tissues. Therefore, we suggest that ATG12 expression in tumor tissues should be further examined. We should also investigate ATG12 expression in different cancer subtypes that are at different stages of the disease. It would be interesting to see if ATG12 expression is dependent on the progression of the cancer.

Next we performed subcellular fractionation and immunoblotting with lung cancer H1299, breast cancer MDA-MA-231 and liver cancer HepG2 cells. After applying mouse and rabbit anti-ATG12 antibodies we could see, that these antibodies detect different ATG12 proteins. With mouse anti-ATG12 antibody we can detect the ATG12 in the mitochondrial fraction, and with rabbit anti-ATG12 antibody we can detect the protein only in the cytosolic fraction. On the film the ATG12 band in mitochondria is visible at a slightly higher molecular weight than the ATG12 band in cytosol. The anti-ATG5 antibody we used, detects the same ATG12-ATG5 conjugate as the rabbit anti-ATG12 antibody. As we

know, the ATG12-ATG5 conjugate is located on the cytosol and it plays a role in the elongation phase of the phagophore. During autophagy it is relocated from the cytosol to the growing autophagosomal membrane (35). By now we know that ATG12, as an ATG12-ATG5 conjugate, may also be located on the mitochondria. Therefore, we assume that at one phase the ATG12-ATG5 conjugate moves from the cytosol to the mitochondria. Based on the different molecular weights of the ATG12-ATG5 conjugate in the mitochondrial and cytosolic fraction, we suspect that at some point it may have undergone some posttranslational modification. Thus the next step would be to identify whether the ATG12-ATG5 conjugate in the mitochondrial fraction is posttranslational modified. The function of the mitochondrial ATG12-ATG5 conjugate has to be explored, as well. Also the trigger and the conditions under which the conjugate is translocated need to be determined.

In addition we could have performed a subcellular fractionation of cells treated with starvation media, chloroquine and a combination of chloroquine in starvation media, followed by immunoblotting with rabbit and mouse anti-ATG12 antibodies. This would have shown if inducing autophagy or blocking it by preventing the fusion of autophagosomes with lysosomes, would also affect cytosolic ATG12 as it does to the mitochondrial ATG12.

Apart from ATG12 playing a role in autophagy, it is also involved in mitochondrial homeostasis and is identified as a pro-apoptotic protein. Besides ATG5, ATG12 also interacts with ATG3 and members of the Bcl-2 family. ATG12 acts as a pro-apoptotic protein by binding Bcl-2; therefore, it is involved in the crosstalk between autophagy and apoptosis. The ATG12 binding mechanism to anti-apoptotic Bcl-2 family proteins differs from that of pro-apoptotic BH3-only proteins; therefore, it could represent a unique way to bind Bcl-2 proteins. This difference could be used as a foundation for further studies on the potential use of ATG12 as a drug target (42).

As mentioned, disruption of ATG12-ATG3 leads to the deregulation of mitochondrial homeostasis, with an increase in mitochondrial mass and resistance to mitochondria mediated apoptosis (44). The exact mechanism of how the ATG12-ATG3 complex regulates mitochondrial homeostasis is still unclear. Therefore, the role of ATG12 in mitochondrial homeostasis should be further investigated, especially the impact of ATG12 on ATP production, mitochondrial DNA and mitochondrial proteins. In ATG12

overexpressing and knockdown cells ATP levels could be measured and compared to wild type cells. Whether ATG12 affects cell viability should also be tested. The main regulators of mitochondrial biogenesis are peroxisome proliferator-activated receptor gamma (PPAR γ) family of proteins, particularly the PGC-1 α which co-activates the NRF2 transcriptional factor. With defective autophagy, NRF2 accumulates in cancer cells, where it promotes cell survival and protects them from oxidative stress (9, 55). Therefore, we propose a future study to investigate the influence of ATG12 on PGC-1 α and other mitochondrial proteins that play an important role in mitochondrial functionality and biogenesis.

6 CONCLUSION

The purpose of this thesis was to further characterize autophagy-related protein 12, an essential protein for autophagic machinery. All experiments were performed with human cell lines.

The hypothesis that ATG12 is located on mitochondria was confirmed by determining co-localization of ATG12 with mitochondrial markers.

Using immunofluorescence microscopy and immunoblotting it was determined that the mitochondrial localization of ATG12 is independent on Bcl-2.

In the colon, mammary gland, prostate, lung, skeletal muscle, esophagus, testicle and stomach tissues, a significantly increased expression of ATG12 was found in tumor tissues in comparison to its corresponding normal tissues.

Next ATG12 was detected by applying mouse and rabbit anti-ATG12 antibodies with immunoblotting. The results indicated a small difference in molecular weight between mitochondrial and cytosolic ATG12-ATG5 conjugates. This suggests that at some point the ATG12-ATG5 conjugate might undergo posttranslational modification.

Autophagy plays an important and very complex role in cancer development. Therefore it is of great importance to further investigate and to gain a better understanding of autophagic machinery. ATG12 and other proteins which regulate autophagy might represent novel biomarkers in the detection and prognosis of cancer and also drug targets in cancer treatment, respectively.

7 REFERENCES

1. Choi MK Augustine, Ryter SW, Levine B: *Autophagy in human health and disease*. The New England Journal of Medicine 2013; 368: 651-62.
2. Levine B, Kroemer G: *Autophagy in the pathogenesis of disease*. Cell 2008; 132: 27-42.
3. Mizushima N: *Autophagy: process and function*. Genes & Development 2007; 21: 2861-2873.
4. Wirawan E, Vanden Berghe T, Lippens S, Agostinis P, Vandenabeele P: *Autophagy: for better or for worse*. Cell Research 2012; 22: 43-61.
5. Mathew R, Karantza-Wadsworth V, White E: *Role of autophagy in cancer*. Nature Reviews – Cancer 2007; 7: 961-967.
6. Rodriguez-Rocha H, Garcia-Garcia A, Panayiotidis MI, Franco R: *DNA damage and autophagy*. Mutation Research/Fundamental and Molecular Mechanisms of Mutagenesis 2011; 711: 158-166.
7. Orvedahl A, Levine B: *Eating the enemy within: autophagy in infectious diseases*. Cell Death and Differentiation 2009; 16: 57-69.
8. Tsujimoto Y, Shimizu S: *Another way to die: autophagic programmed cell death*. Cell Death and Differentiation 2005; 12: 1528-1534.
9. Liu H, He Z, Simon HU: *Targeting autophagy as a potential therapeutic approach for melanoma therapy*. Seminars in Cancer Biology 2013; 23: 352-360.
10. White E: *Deconvoluting the context-dependent role for autophagy in cancer*. Nature Reviews - Cancer 2012; 12: 401-410.
11. Chen N, Debnath J: *Autophagy and tumorigenesis*. FEBS letters 2010; 584: 1427-1435.
12. Jaramillo MC, Zhang DD: *The emerging role of the Nrf2-Keap1 signaling pathway in cancer*. Genes & Development 2013; 27: 2179-2191.
13. Degenhardt K, Mathew R, Beaudoin B, Bray K, Anderson D, Chen G, Mukherjee C, Shi Y, Gélinas C, Fan Y, Nelson DA, Jin S, White E: *Autophagy promotes tumor cell survival and restricts necrosis, inflammation and tumorigenesis*. Cancer Cell 2006; 10: 51-64.
14. Janji B, Viry E, Baginska J, Van Moer K, Berchem G: *Autophagy - A Double-Edged Sword - Cell Survival or Death?*, Intech, 2013: 189-215.

15. Narita M, Young AR, Narita M: *Autophagy facilitates oncogene-induced senescence*. *Autophagy* 2009; 5: 1046-1047.
16. Paoli P, Giannoni E, Chiarugi P: *Anoikis molecular pathways and its role in cancer progression*. *Biochimica et Biophysica Acta* 2013; 1833: 3481-3498.
17. Di Bartolomeo S, Corazzari M, Nazio F, Oliverio S, Lisi G, Antonioli M, Pagliarini V, Matteoni S, Fuoco C, Giunta L, D'Amelio M, Nardacci R, Romagnoli A, Piacentini M, Cecconi F, Fimia GM: *The dynamic interaction of AMBRA1 with the dynein motor complex regulates mammalian autophagy*. *The Journal of Cell Biology* 2010; 191: 155-168.
18. Wirth M, Joachim J, Tooze SA: *Autophagosome formation - the role of ULK1 and Beclin1-PI3KC3 complexes in setting the stage*. *Seminars in Cancer Biology* 2013; 23: 301-309.
19. Chen Y, Klionsky DJ: *The regulation of autophagy - unanswered questions*. *Journal of Cell Science* 2011; 124: 161-170.
20. Glick D, Barth S, Macleod KF: *Autophagy: cellular and molecular mechanisms*. *The Journal of Pathology* 2010; 221: 3-12.
21. Dunlop EA, Tee AR: *mTOR and autophagy: A dynamic relationship governed by nutrients and energy*. *Seminars in Cell & Developmental Biology* 2014; 36: 121-129.
22. Feng Y, He D, Yao Z, Klionsky DJ: *The machinery of macroautophagy*. *Cell Research* 2014; 24: 24-41.
23. Badadani M: *Autophagy Mechanism, Regulation, Functions, and Disorders*. *ISRN Cell Biology* 2012; 2012.
24. Shpilka T, Mizushima N, Elazar Z: *Ubiquitin-like proteins and autophagy at a glance*. *Journal of cell science* 2012; 125: 2343-8.
25. Xie Z, Nair U, Klionsky DJ: *Atg8 controls phagophore expansion during autophagosome formation*. *Molecular Biology of the Cell* 2008; 19: 3290-3298.
26. Hale AN, Ledbetter DJ, Gawriluk TR, Rucker EB: *Regulation and role in development*. *Autophagy* 2013; 9: 951-972.
27. Helgason GV, Karvela M, Holyoake TL: *Kill one bird with two stones: potential efficacy of BCR-ABL and autophagy inhibition in CML*. *Blood* 2011; 118: 2035-43.
28. Cheng Y, Ren X, Hait WN, Yang JM: *Therapeutic targeting of autophagy in disease: biology and pharmacology*. *Pharmacological reviews* 2013; 65: 1162-97.

29. Kimura T, Takabatake Y, Takahashi A, Isaka Y: *Chloroquine in cancer therapy: a double-edged sword of autophagy*. Cancer Research 2013; 73: 3-7.
30. Liang X, Tang J, Liang Y, Jin R, Cai X: *Suppression of autophagy by chloroquine sensitizes 5-fluorouracil-mediated cell death in gallbladder carcinoma cells*. Cell & Bioscience 2014; 4: 10.
31. Choi YJ, Park YJ, Park JY, Jeong HO, Kim DH, Ha YM, Kim JM, Song YM, Heo HS, Yu BP, Chun P, Moon HR, Chung HY: *Inhibitory Effect of mTOR Activator MHY1485 on Autophagy: Suppression of Lysosomal Fusion*. Plos ONE 2012; 7: e43418.
32. Tanemura M, Ohmura Y, Deguchi T, Machida T, Tsukamoto R, Wada H, Kobayashi S, Marubashi S, Eguchi H, Ito T, Nagano H, Mori M, Doki Y: *Rapamycin causes upregulation of autophagy and impairs islets function both in vitro and in vivo*. American Journal of Transplantation 2012; 12: 102-114.
33. <http://www.genecards.org/cgi-bin/carddisp.pl?gene=ATG12>, available in October 2014.
34. Yang Z, Klionsky DJ: *An overview of the molecular mechanism of autophagy*. Current topics in microbiology and immunology 2009; 335: 1-32.
35. Otomo C, Metlagel Z, Takaesu G, Otomo T: *Structure of the human ATG12-ATG5 conjugate required for LC3 lipidation in autophagy*. Nature structural & molecular biology 2013; 20: 59-66.
36. Ravikumar B, Futter M, Jahreiss L, Korolchuk VI, Lichtenberg M, Luo S, Massey DC, Menzies FM, Narayanan U, Renna M, Jimenez-Sanchez M, Sarkar S, Underwood B, Winslow A, Rubinsztein DC: *Mammalian macroautophagy at a glance*. Journal of Cell Science 2009; 122: 1707-11.
37. Elmore S: *Apoptosis: A Review of Programmed Cell Death*. Toxicologic Pathology 2007; 35: 495-516.
38. Wong RS: *Apoptosis in cancer: from pathogenesis to treatment*. Journal of Experimental & Clinical Cancer Research 2001; 30.
39. Hardwick JM, Soane L: *Multiple functions of BCL-2 family proteins*. Journal of Experimental & Clinical Cancer Research 2014; 5.
40. Petros AM, Olejniczak ET, Fesik SW: *Structural biology of the Bcl-2 family of proteins*. Biochimica et Biophysica Acta 2004; 1644: 83-94.

41. Braun F, de Carné Trécesson S, Bertin-Ciftci J, Juin P: *Protect and serve: Bcl-2 proteins as guardians and rulers of cancer cell survival*. Cell Cycle 2013; 12: 2937-2947.
42. Rubinstein AD, Eisenstein M, Ber Y, Bialik S, Kimchi A: *The autophagy protein Atg12 associates with antiapoptotic Bcl-2 family members to promote mitochondrial apoptosis*. Molecular cell 2011; 44: 698-709.
43. Chonghaile TN, Letai A: *Who Put the “A” in Atg12: Autophagy or Apoptosis?* Molecular cell 2011; 44: 844–845.
44. Radoshevich L, Murrow L, Chen N, Fernandez E, Roy S, Fung C, Debnath J: *ATG12 conjugation to ATG3 regulates mitochondrial homeostasis and cell death*. Cell 2010; 142: 590-600.
45. Radoshevich L, Debnath J: *ATG12–ATG3 and mitochondria*. Autophagy 2011; 7: 109-111.
46. Liu H, He Z, von Rütte T, Yousefi S, Hunger RE, Simon HU: *Down-regulation of autophagy-related protein 5 (ATG5) contributes to the pathogenesis of early-stage cutaneous melanoma*. Science translational medicine 2013; 5: 202ra123.
47. Kuma A, Hatano M, Matsui M, Yamamoto A, Nakaya H, Yoshimori T, Ohsumi Y, Tokuhiya T, Mizushima N: *The role of autophagy during the early neonatal starvation period*. Nature 2004; 432: 1032-1036.
48. Maskey D, Yousefi S, Schmid I, Zlobec I, Perren A, Friis R, Simon HU: *ATG5 is induced by DNA-damaging agents and promotes mitotic catastrophe independent of autophagy*. Nature communications 2013; 4: 2013.
49. Germič N: *Subcellular localization of autophagy-related protein 12*. Master thesis 2014, Faculty of Pharmacy, University of Ljubljana.
50. <http://www.genecards.org/cgi-bin/carddisp.pl?gene=SSBP1>, available in November 2014.
51. Youle RJ, Strasser A: *The BCL-2 protein family: opposing activities that mediate cell death*. Nature Reviews Molecular Cell Biology 2008; 9: 47-59.
52. Martin SJ, Reutelingsperger CP, McGahon AJ, Rader JA, van Schie RC, LaFace DM, Green DR: *Early redistribution of plasma membrane phosphatidylserine is a general feature of apoptosis regardless of the initiating stimulus: inhibition by overexpression of Bcl-2 and Abl*. The journal of experimental medicine 1995; 182: 1545-56.

53. Jawhar NM: *Tissue Microarray: A rapidly evolving diagnostic and research tool.* Annals of Saudi medicine 2009; 29: 123-7.
54. Mizushima N, Yoshimori T: *How to interpret LC3 immunoblotting.* Autophagy 2007; 3: 542-5.
55. Sporn MB, Liby KT: *NRF2 and cancer: the good, the bad and the importance of context.* Nature reviews - cancer 2012; 12: 564-71.